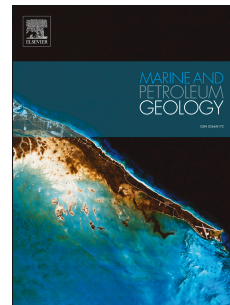


Journal Pre-proof

Vertical effective stress and temperature as controls of quartz cementation in sandstones: Evidence from North Sea fulmar and Gulf of Mexico Wilcox sandstones

Olakunle J. Oye, Andrew C. Aplin, Stuart J. Jones, Jon G. Gluyas, Leon Bowen, Joseph Harwood, Ian J. Orland, John W. Valley



PII: S0264-8172(20)30072-6

DOI: <https://doi.org/10.1016/j.marpetgeo.2020.104289>

Reference: JMPG 104289

To appear in: *Marine and Petroleum Geology*

Received Date: 10 September 2019

Revised Date: 22 January 2020

Accepted Date: 7 February 2020

Please cite this article as: Oye, O.J., Aplin, A.C., Jones, S.J., Gluyas, J.G., Bowen, L., Harwood, J., Orland, I.J., Valley, J.W., Vertical effective stress and temperature as controls of quartz cementation in sandstones: Evidence from North Sea fulmar and Gulf of Mexico Wilcox sandstones, *Marine and Petroleum Geology* (2020), doi: <https://doi.org/10.1016/j.marpetgeo.2020.104289>.

This is a PDF file of an article that has undergone enhancements after acceptance, such as the addition of a cover page and metadata, and formatting for readability, but it is not yet the definitive version of record. This version will undergo additional copyediting, typesetting and review before it is published in its final form, but we are providing this version to give early visibility of the article. Please note that, during the production process, errors may be discovered which could affect the content, and all legal disclaimers that apply to the journal pertain.

© 2020 Published by Elsevier Ltd.

Ms. Ref. No.: JMPG-D-19-01119

Title: Vertical Effective Stress and Temperature as Controls of Quartz Cementation in Sandstones:
Evidence from North Sea Fulmar and Gulf of Mexico Wilcox Sandstones
Marine and Petroleum Geology

Authors: Olakunle J. Oye, Andrew C. Aplin, Stuart J. Jones, Jon G. Gluyas, Leon Bowen, Joseph Harwood, Ian J. Orland, and John W. Valley

We certify that all authors have seen and approved the final version of the manuscript being submitted. We warrant that the article is the authors' original work, hasn't received prior publication and isn't under consideration for publication elsewhere.

Journal Pre-proof

1 **Vertical Effective Stress and Temperature as Controls of Quartz**
2 **Cementation in Sandstones: Evidence from North Sea Fulmar and Gulf**
3 **of Mexico Wilcox Sandstones**

4
5 **Olakunle J. Oye¹, Andrew C. Aplin^{1*}, Stuart J. Jones¹, Jon G. Gluyas¹, Leon Bowen², Joseph**
6 **Harwood³, Ian J. Orland⁴, and John W. Valley⁴**

7
8 ¹Department of Earth Sciences, Durham University, Durham, DH1 3LE, UK

9 ²Department of Physics, Durham University, Durham, DH1 3LE, UK

10 ³School of Geography, University of Lincoln, Lincoln, LN6 7TS, UK

11 ⁴WiscSIMS Lab, Department of Geoscience, University of Wisconsin, Madison, WI, 53706-
12 1692, USA

13 **ABSTRACT**

14 We present quantitative petrographic data, high spatial resolution oxygen isotope analyses of quartz
15 cement, basin modelling and a kinetic model for quartz precipitation for two Paleocene-Eocene
16 Wilcox Group sandstones from Texas and two Jurassic Fulmar Formation sandstones from the
17 Central North Sea. At each location, one sandstone has been buried to *ca.* 145 °C and one to *ca.* 185
18 °C. A key difference between the Wilcox and Fulmar burial histories is that the Wilcox sandstones
19 are currently at higher vertical effective stresses and, from basin modelling studies, have been
20 subjected to generally higher vertical effective stresses through their burial history. The amounts of

21 quartz cement in the Wilcox sandstones are between 12 and 18%, and between 2 and 6% in the
22 Fulmar sandstones. High-spatial-resolution oxygen isotope data obtained from the quartz cements
23 suggest temperature ranges for quartz precipitation from 60-80 °C to values approaching maximum
24 burial temperature. Factors such as grain coatings or the timing of petroleum emplacement cannot
25 explain the differences in the amounts of quartz cement. Petrographic data show that most of the
26 silica for quartz cement can be derived from intergranular pressure dissolution. Although the sample
27 set is small, we interpret the results to suggest that the differences in quartz cementation in Fulmar
28 and Wilcox sandstones can be explained better by differences in their vertical effective stress history
29 than their temperature history; in this case, the supply of silica rather than the precipitation of
30 quartz becomes an important control on the rate and extent of cementation.

31

32 Keywords: Sandstone; Diagenesis; Quartz cement; Effective stress; Intergranular pressure
33 dissolution; Secondary ion mass spectrometry; Oxygen isotopes

34

35

36 **1 INTRODUCTION**

37 Quartz is the volumetrically most important diagenetic cement in sandstones buried to depths
38 greater than 2.5 km (Bjorlykke and Egeberg, 1993; McBride, 1989; Worden et al., 2018a; Worden
39 and Morad, 2000). Quartz cementation occurs as the result of three serially linked processes: the
40 supply of silica; the transport of silica through aqueous solution to precipitation sites; and the
41 precipitation of quartz cement (e.g. Bloch et al., 2002; Taylor et al., 2010; Worden and Morad, 2000).
42 While any of these processes could be the rate-controlling step (e.g. Osborne and Swarbrick, 1999;
43 Oye et al., 2018; Robinson and Gluyas, 1992; see Sheldon et al., 2003; Walderhaug, 1996; Worden et
44 al., 2018b; Worden and Morad, 2000), the currently favoured paradigm is that quartz cementation is
45 controlled by the temperature-related kinetics of silica precipitation (Lander and Walderhaug, 1999;
46 Walderhaug, 1996, 2000). In this model, quartz precipitation initiates on geological timescales once
47 a kinetic barrier is broken around 70 – 80 °C, with the rate increasing exponentially and predictably
48 with temperature (Ajdukiewicz and Lander, 2010; Walderhaug, 1994a, 1996). These ideas have been
49 incorporated into commonly-used models designed to predict quartz cementation and reservoir
50 quality, allowing quartz cementation to be predicted as a function of temperature history (Lander et
51 al., 2008; Lander and Walderhaug, 1999; Taylor et al., 2015; Walderhaug, 2000).

52 The critical assumption in the temperature-based precipitation model is that silica supply is
53 effectively inexhaustible, so that for each silica molecule precipitated, another is released from a
54 range of potential sources. The most commonly cited and observed silica source is from
55 intergranular pressure dissolution and related stylolitisation at quartz-quartz and quartz-sheet
56 silicate interfaces (Houseknecht, 1988; Osborne and Swarbrick, 1999; Pittman, 1972; Waldschmidt,
57 1941; Worden and Morad, 2000). In one variant of this model, Bjorkum (1996) proposed that silica is

58 derived from pressure-*insensitive* dissolution at quartz-mica interfaces, in which case the rate of
59 quartz cementation is controlled uniquely by temperature-related precipitation kinetics.

60 More commonly, the rate of intergranular pressure dissolution is considered to be primarily a
61 function of vertical effective stress, with a secondary influence of temperature (e.g. van Noort et al.,
62 2008); it occurs at grain contacts because the chemical potential of silica at stressed, grain-grain
63 contacts is enhanced over that in the bulk solution. Gradients in chemical potential drive
64 intergranular pressure dissolution and releases silica which can then precipitate on free detrital
65 quartz surfaces (De Boer et al., 1977; Dewers and Ortoleva, 1990; Elias and Hajash, 1992; Gratier et
66 al., 2005; Oye et al., 2018; Renard et al., 1997; Sheldon et al., 2003; Shimizu, 1995; Tada and Siever,
67 1989; van Noort et al., 2008). If (a) the silica for quartz cementation was supplied primarily from
68 intergranular pressure dissolution, and (b) supply rather the precipitation is the rate-controlling step
69 for quartz cementation, we would expect to see a relationship between the extent and rate of
70 cementation with the history of vertical effective stress, rather than temperature. Such a
71 relationship has been proposed previously (Elias and Hajash, 1992; Osborne and Swarbrick, 1999;
72 Sheldon et al., 2003) but rarely tested (Oye et al., 2018).

73 There are other, local influences on quartz cementation which can complicate the evaluation of the
74 relative importance of silica supply or precipitation as master cementation variables. Grain-coating
75 clay and microquartz reduce the availability of precipitation sites on quartz grains, inhibiting
76 cementation and preserving porosity (Aase et al., 1996; Ajdukiewicz et al., 2010; Bloch et al., 2002;
77 French et al., 2012; Gluyas et al., 1993; Heald and Larese, 1974; Osborne and Swarbrick, 1999;
78 Stricker and Jones, 2016; Stricker et al., 2016). Furthermore, although debate continues, there is
79 some consensus that the occurrence of hydrocarbons slows the rate of quartz cementation by
80 altering the wetting state of grains and/or increasing the tortuosity of diffusion pathways (Maast et
81 al., 2011; Marchand et al., 2000; Marchand et al., 2001; Marchand et al., 2002; Sathar et al., 2012;
82 Worden et al., 2018b).

83 The aim of this paper is to consider the relative importance of (a) silica supply by intergranular
84 pressure dissolution, and (b) silica precipitation as controls on quartz cementation. In an earlier
85 paper, Oye et al. (2018) described the anomalously low volumes of quartz cement in sandstones
86 from the North Sea's High Pressure High Temperature Elgin field, suggesting that it may be the
87 history of effective stress rather than the history of temperature which is a key control on quartz
88 cementation. Here, we extend that study and test its findings more robustly by studying four
89 carefully selected sandstones that have different vertical effective stress and temperature histories.
90 Two were chosen from Upper Jurassic Fulmar Formation sandstones from Clyde and (the previously
91 studied) Elgin Fields in the Central North Sea (CNS), UK, and two from Paleocene-Eocene Wilcox
92 Group sandstones from Rotherwood and Lake Creek Fields in the Texas coast, Gulf of Mexico (GoM),
93 USA (Fig. 1); Elgin and Rotherwood have lower present-day vertical effective stress and higher
94 temperatures than their equivalents from Clyde and Lake Creek (Table 1). Our approach is to
95 integrate (a) quantitative petrographic analysis, (b) basin modelling to evaluate temperature and
96 vertical effective stress histories, (c) high-spatial-resolution oxygen isotope analyses to evaluate
97 quartz cementation histories and (d) kinetic modelling of quartz cementation.

98

99 **2 GEOLOGICAL SETTINGS**

100 Samples were selected from four locations, two from the UK North Sea and two from the Texas Gulf
101 Coast, enabling us to examine the relative importance of both temperature and vertical effective
102 stress on quartz cementation (Table 1). For the chosen Formations, Elgin (North Sea) and
103 Rotherwood (Texas) have current temperatures of 185-189°C but different vertical effective stress,
104 and Clyde (North Sea) and Lake Creek (Texas) have temperatures of 143-147°C, again with different
105 vertical effective stress.

106 Samples from Elgin and Clyde fields were taken from the syn-rift Upper Jurassic Fulmar Formation in
107 the Central Graben area of the UK North Sea (Fig. 1). The Upper Jurassic Fulmar Formation is one of
108 the principal hydrocarbon reservoirs in the UK Central Graben (e.g. Gilham et al., 2005; Gowland,
109 1996; Kuhn et al., 2003; Lasocki et al., 1999; Osborne and Swarbrick, 1999; Stevens and Wallis, 1991;
110 Wilkinson and Haszeldine, 2011; Wilkinson et al., 2006). Sediments were probably sourced from the
111 Triassic sedimentary rocks of the Western Platform in the Central North Sea, with some
112 contributions from intrabasinal highs such as the Forties – Montrose High and Josephine ridge
113 (Gowland, 1996). The Fulmar Formation is a shallow marine sandstone, intensely bioturbated and
114 often occurring as a coarsening-upward succession grading from siltstones into very fine to medium
115 grained arkosic sandstones (Gowland, 1996; Hendry et al., 2000; Lasocki et al., 1999). The Fulmar
116 Formation is mainly Oxfordian to Kimmeridgian in age, but its geographic variability and diachroneity
117 resulted in the occurrence of localised areas of the Fulmar Formation with younger ages that extend
118 to Ryazanian times (Fig. 2). The presence of abundant *Rhaxella* sponge spicules has been reported
119 within some intervals, locally (Gowland, 1996). The Fulmar Formation is buried beneath a thick
120 Upper Jurassic to Tertiary succession of chalk, clays and silts.

121 Samples from the upper Texas Gulf Coast were taken from the Late Paleocene to Early Eocene,
122 fluvio-deltaic Wilcox Group (Fig. 1 and Fig. 3 (Dutton and Loucks 2010; Fisher and McGowen 1967;
123 Galloway et al. 2000)). Wilcox Group sediments comprise a series of sandstones, siltstones and
124 shales which have been extensively studied (Dutton and Loucks, 2010; Fisher and McGowen, 1967;
125 Galloway et al., 2000). Sediments were likely sourced from the Laramide uplands area in the
126 southern Rocky Mountains. Most Wilcox sandstones in the upper Texas coast are lithic arkoses and
127 feldspathic litharenites (Dutton and Loucks, 2010). Because geothermal gradients vary in the Texas
128 coast area from 24 to 43°C/km, the Wilcox sandstones exhibit varying temperature regimes across
129 different localities (Dutton and Loucks, 2010).

130 **3 METHODS**

131 **3.1 Sampling Strategy**

132 A key objective of this paper is consider the relative importance of effective stress and temperature
133 histories as controls on quartz cementation in sandstones. Since other factors, some of which vary
134 on small spatial scales, also influence the amount of quartz cement (grain-coating clay, early
135 carbonate cement, grain-coating microquartz, hydrocarbon fill in the porosity), our sampling
136 strategy here was to obtain a relatively small number of samples with a limited range of detrital
137 mineralogy and grain size. Restricting the influence of other variables allows greater insights into the
138 importance of effective stress and temperature histories. Furthermore, our aim to constrain quartz
139 cementation histories based on oxygen isotope microanalysis using secondary ion mass
140 spectrometry, inevitably restricts the number of samples which can be characterised in detail.

141 Fulmar Formation samples were obtained from wells 30/17b-2 and 22/30c-G4 in Clyde and Elgin
142 Fields respectively (Fig. 1), from clean, clay-poor intervals (Table 1). A similar strategy was adopted
143 for the Wilcox sandstones: two wells that penetrated the Wilcox sandstones were selected, one
144 from Mobil #48 well in Lake Creek Field, Montgomery County, and one from Texaco #1 well in
145 Rotherwood Field, Harris County, Texas. All the sandstones are at or close to their maximum burial
146 depth. Sample depths, temperatures and vertical effective stress are given in Table 1.

147 **3.2 Petrography**

148 Petrographic data for the Wilcox sandstones were obtained from Harwood (2011), except
149 intergranular pressure dissolution data which were measured in this study. Fulmar Formation
150 sandstones were characterised using standard and cathodoluminescence (SEM-CL) petrography.
151 Using a standard petrographic microscope, grain types, matrix and cement contents were quantified
152 by making not less than 300 point counts per thin section. This revealed that some Fulmar samples
153 contained early carbonate cement. These carbonate cement-rich samples were excluded from
154 further analyses, since early carbonate can significantly occlude porosity and thus bias quartz

155 cement results. Twenty Fulmar samples (Table S6), representing the full range of quartz cement
156 abundance, were subsequently selected for CL petrography. The CL petrography involved the
157 acquisition of Si element and CL maps over the same areas (3mm x 3mm) for each of the twenty thin
158 sections using energy dispersive X-ray (EDX) and SEM-CL. A grid of 1600 (40x40) square boxes was
159 superimposed on the CL map, while the EDX map was used as a control for the identification of
160 mineral grains. Modal analysis was then performed by manually point-counting detrital quartz,
161 dissolved quartz along grain contacts and authigenic quartz using the grids to generate 1600 data
162 points per thin section. Cathodoluminescence petrography allows discrimination of original grains
163 and cements, so that initial grain sizes were estimated by measuring the diameter of ~ 120 grains
164 each from ten Fulmar thin-sections. A more detailed CL petrography method is described in the
165 supplementary material.

166 **3.3 Effective Stress and Temperature Histories**

167 One-dimensional basin modelling was used in this study to reconstruct the burial, pore pressure,
168 effective stress and temperature histories for both Fulmar Formation and Wilcox Group sandstones
169 using Schlumberger's PetroMod Petroleum Systems modelling software (Version 2014.1).

170 Stratigraphic data from composite logs, geological well reports, core analysis, and core description
171 reports were used to create the models (Tables S1, S2 and S3). Drill Stem Test (DST) temperature
172 data for Clyde field obtained from well composite log and corrected bottom-hole temperature (BHT)
173 data for Elgin field were obtained from unpublished well reports. Historical mean surface
174 temperatures were estimated using an PetroMod inbuilt algorithm that relates global mean surface
175 temperatures with paleolatitudes and geologic ages. Heat flow models were built after Allen and
176 Allen (1990), with an average of 62 and 64 mW/m² for Elgin and Clyde fields through the basin's
177 history. The heat flow values at the peak of Permo-Triassic and Upper Jurassic paleo-rifting events
178 were 70 and 90 mW/m² respectively for both Elgin and Clyde fields. Heat flow, however, averages
179 ~57 mW/m² (range 50 - 78 mW/m²) for fields in the Gulf of Mexico (Nunn and Sassen, 1986; Smith
180 et al., 1981). Vitrinite reflectance data (only available for the Fulmar sandstones) were used as

181 paleothermometers and combined with present-day temperature data to constrain thermal models
182 and reconstruct temperature evolution through time (Figure S1, S2, S3 and S4).

183 For the fluid flow part of the basin modelling, lithological data for each sedimentary unit were
184 defined in Clyde and Elgin Fields from well composite logs and core analysis descriptions, while the
185 lithologies for Lake Creek and Rotherwood Fields were solely based on log data. Petromod's default
186 lithologies were modified to match those observed in field samples. Pore pressure data obtained
187 from field measurements were used to constrain the pore pressure model for reconstruction of
188 effective stress histories for all the fields. The calculation of vertical effective stress is based on the
189 mathematical expression of Terzaghi (1925):

$$\sigma_v = S_v - P \quad (1)$$

190 where σ_v is vertical effective stress, S_v is vertical lithostatic stress and P is pore fluid pressure (all in
191 Pa).

192 Default chalk and shale permeabilities in PetroMod were modified after Swarbrick et al. (2000),
193 lowering permeabilities for the Chalk Group and the Pre-Cretaceous shale units until a good fit was
194 achieved between modelled and observed pore pressures. The Chalk group were assigned typical
195 shale permeability values because they are extensively cemented (Swarbrick et al., 2000; Swarbrick
196 et al., 2010). Similar adjustments were made for Rotherwood and Lake Creek fields, where
197 permeability values for the Claiborne and Wilcox shales were modified to lower values (nanoDarcies)
198 until modelled pore pressures matched field data.

199 Although temperature histories can be quite accurately modelled in 1D, the same is not necessarily
200 true for pore pressure and vertical effective stress, since one-dimensional modelling packages are
201 limited by their inability to model lateral fluid flow. It transpires that this is critical for the Clyde field,
202 where regional pore pressure data within the Fulmar Formation show that pore fluid pressures have
203 decreased substantially in the last *ca.* 0.5 million years as a result of lateral drainage (Swarbrick et

204 al., 2005). These data strongly suggest that vertical effective stress has increased from *ca.* 19 MPa
 205 0.5 million years ago, to 40 MPa at the present-day. This is critical for the present study, given its
 206 focus on unravelling the relative importance of temperature and effective stress on quartz
 207 cementation.

208

209 **3.4 Kinetic Model of Quartz Cementation**

210 Quartz cementation models were built using Walderhaug's (1996) approach, which simulates the
 211 precipitation of silica on quartz surfaces as a logarithmic function of temperature. Commercial
 212 quartz cementation modelling software packages based on the Arrhenius equation have also been
 213 developed (e.g. Lander et al., 2008; Walderhaug, 2000; Walderhaug et al., 2000) but were not
 214 available for this study. However, the essential inputs for each model - a time-temperature history
 215 and the surface area of macroquartz grains - are the same. The key difference is that in the
 216 Walderhaug (1996) model, the kinetics of precipitation are defined by a logarithmic function,
 217 whereas in the Arrhenius approach, the kinetics are defined by the pre-exponential factor and
 218 activation energy terms in the Arrhenius equation. In both cases, key kinetic parameters can be
 219 adjusted to obtain local calibrations to quartz cement abundances. Local calibration is not the aim
 220 here; rather, we use single values of the key kinetic constants in Walderhaug's (1996) equation to
 221 observe the extent to which a general model can match observed amounts of quartz cement in
 222 different settings. Whilst the Arrhenius approach to the quantification of quartz precipitation may
 223 have a more robust scientific basis, we note that Arrhenius and logarithm-based methods yielded
 224 similar results for some Jurassic Brent Group sandstones from the North Sea (Walderhaug, 2000).

225 Walderhaug's (1996) empirical model is mathematically expressed as:

$$Vq_2 = \Phi_0 - (\Phi_0 - Vq_1) \exp \frac{-MaA_0}{\rho\Phi_0bc \ln 10} (10^{bT_2} - 10^{bT_1}) \quad (2)$$

226 where M and ρ are molar mass (60.09 g/mol) and density (2.65g/cm³) of quartz; c is the heating
227 rate (°C/s) calculated from time-temperature history; ϕ_0 is the porosity at the onset of precipitation;
228 Vq_1 is the volume (cm³) of quartz cement present in 1 cm³ of sandstone at time T_1 (s); Vq_2 is the
229 volume (cm³) of quartz cement precipitated in 1 cm³ of sandstone from time T_1 and T_2 (s); A_0 is initial
230 quartz surface area (cm²) in 1 cm³ of sandstone (estimated from grain size); and a (moles/cm²s) and
231 b (°C⁻¹) are the precipitation kinetic constants (Walderhaug, 1996).

232 Through the quartz surface area term, the model incorporates grain size, mineralogy, and available
233 quartz surface area, all of which were quantified in this study. The model assumes that compaction
234 terminates at the onset of quartz cementation, at which point the sandstone framework is stabilised.
235 Time-temperature histories generated from Petromod were used to calculate the heating rates
236 incorporated in the cementation models. The model used 1cm³ sandstone, an 80°C threshold
237 temperature for cementation, 26% porosity at the onset of quartz cementation, grain size estimates
238 from thin-sections during CL petrography, and Walderhaug's (1994b) kinetic constants a (1.98×10^{-22}
239 moles/cm²s) and b (0.022°C⁻¹). Fractions of detrital quartz in the bulk rock were obtained from CL
240 petrographic data. Quantitative petrographic data of grain coat coverage were also incorporated in
241 the model using a method similar to Walderhaug's (1996) and (Walderhaug, 2000) approach, for a
242 better constraint of the available quartz surface area. Quantification of grain coatings coverage was
243 done through visual inspection and manual point counting using cathodoluminescence, back-
244 scattered electron, and silica maps generated over the same area (Oye et al., 2018). While back-
245 scattered electron microscopy allowed the identification of microquartz and clay coatings in thin
246 section, cathodoluminescence and silica maps helped identify and discriminate quartz grains and
247 cement.

248 **3.5 Oxygen Isotope Analysis**

249 One sample was selected from each of Clyde and Elgin fields for *in situ* oxygen isotope analysis of
250 quartz overgrowths, using a CAMECA IMS-1280 ion microprobe at the WiscSIMS Laboratory at the
251 University of Wisconsin-Madison (Kelly et al., 2007; Kita et al., 2009; Valley and Kita, 2009). Six

252 overgrowths with thicknesses between 40 and 100 μm , three from each sandstone sample, were
253 chosen for analysis. Linear profiles of $\delta^{18}\text{O}$ were measured across each overgrowth using a $3\mu\text{m}$ spot
254 diameter. Individual samples were embedded in a polished epoxy mount alongside grains of
255 University of Wisconsin quartz standard UWQ-1 (Kelly et al., 2007). Bracketing analyses were
256 performed on the quartz standard grains within each of the mounts to enable correction of
257 measured $\delta^{18}\text{O}$ values to the Vienna Standard Mean Ocean Water (VSMOW) scale. Normally, eight
258 UWQ-1 analyses bracketed each group of ~ 12 sample analyses to monitor instrumental drift and to
259 calculate external reproducibility for sample analyses (Kita et al., 2009; Valley and Kita, 2009). The
260 average spot-to-spot reproducibility of $\delta^{18}\text{O}$ in the bracketing UWQ1 analyses was 0.7‰ (2 standard
261 deviations).

262 Ion microprobe analysis of individual quartz overgrowths in Wilcox and Fulmar sandstones were
263 similar except that measurements in the Wilcox sandstones were made using a $12\mu\text{m}$ spot size,
264 which improved spot-to-spot reproducibility to $0.X\text{‰}$ (2 standard deviations). In addition, 16OH^- was
265 measured simultaneously during $\delta^{18}\text{O}$ analysis of the Fulmar samples. Ratios of $16\text{OH}^-/16\text{O}^-$ were
266 background-corrected by subtraction of average ratios measured on nominally anhydrous UWQ-1
267 analyses that bracketed each block of sample data. Four analyses representing outlying data points
268 after $16\text{OH}^-/16\text{O}^-$ correction were discarded (Fig. S4 and Fig.S5). A more detailed ion microprobe
269 analytical procedure is described in prior studies (Kita et al., 2009; Oye et al., 2018; Page et al., 2007;
270 Pollington et al., 2011; Valley and Kita, 2009). All data are reported in the supplementary material
271 (Table S8 and S9).

272 **4 RESULTS**

273 **4.1 Burial, Temperature and Vertical Effective Stress Histories**

274 Burial histories are shown in Figure 4, and both temperature and vertical effective stress histories in
275 Figure 5. Temperature histories for Clyde and Elgin fields are broadly similar, with higher

276 temperatures in Elgin as a result of a more rapid early phase of burial (Fig.5). Temperature histories
277 for Rotherwood and Lake Creek fields are also like each other, with higher temperatures in
278 Rotherwood field due to greater burial in the Eocene-Oligocene (Fig. 5).

279 In Rotherwood and Lake Creek fields, vertical effective stress increases rapidly in the first 10-20
280 million years as a result of the rapid burial of a relatively coarse-grained sedimentary sequence
281 which allows the effective dissipation of fluid overpressure (Fig. 5). Vertical effective stress is then
282 fairly constant until the present-day. Although the Wilcox Group at Lake Creek field is less deeply-
283 buried than at Rotherwood field, vertical effective stress is higher as fluid pressure is much lower,
284 reflecting the more rapid burial at Rotherwood field and the relative inability of the sediment
285 sequence to dewater and thus lose pore pressure at the same rate as it is being generated by
286 additional sediment loading.

287 Vertical effective stress is low in the Fulmar Formation throughout the burial history of Elgin field,
288 and was never greater than the present 12 MPa (Fig. 5). This is due to the fine-grained nature and
289 low permeability of most of the overburden above the Fulmar sandstones (See Supplementary
290 Material). Since the stratigraphic column at Clyde field is like that at Elgin, the evolution of vertical
291 effective stress should be similar to that at Elgin, perhaps with slightly higher vertical effective stress
292 due to a lower burial rate and thus the greater possibility of pore pressure dissipation by fluid flow.
293 However, the present-day vertical effective stress is much higher than that at Elgin, 40 MPa rather
294 than 12 MPa (Table 1). As discussed earlier, regional studies of the Fulmar Formation in the Clyde
295 area show pore pressure distributions which indicate regional depressurisation of the Fulmar
296 sandstones through a leak point well to the west of Clyde (Swarbrick et al., 2005). The regional pore
297 pressure data are best interpreted as depressurisation occurring over the last 0.5 million years,
298 increasing the vertical effective stress at Clyde from 19 MPa to 40 MPa (Swarbrick et al., 2005).
299 Vertical effective stress at Clyde is likely to have been low, no more than 19 MPa, throughout all of
300 its burial history bar the last 0.5 Ma.

301

302 **4.2 Petrographic Observations**

303 The two Wilcox sandstone samples from Rotherwood and Lake Creek fields are clean, fine grained,
304 lithic sub-arkose sandstones, with higher plagioclase fractions than their Fulmar Formation
305 counterparts (Fig. 6; Table 2 and Table 3). Average porosities in the examined samples are 6.8% for
306 the sample from the Texaco #1 Hallson well in Rotherwood field and 11.8% for the sample from the
307 Mobil #48 well in Lake Creek field (Table 3). The feldspars have experienced large scale albitization
308 and dissolution (Dutton and Loucks, 2010). Grain-replacing-ankerite cements were observed only in
309 the sample from the higher-temperature Rotherwood Field (Fig. 6E).

310 The Upper Jurassic Fulmar Formation sandstones investigated in this study were selected from clay-
311 poor, upper shoreface facies in Clyde and Elgin Fields. They are fine grained, with subangular to
312 subrounded grains, and an arkosic mineralogical composition. Illite, the main authigenic clay type
313 observed in these sandstones, is generally less than 3% of bulk composition in all thin sections (Table
314 2). These clays most likely have both detrital and authigenic (product of feldspar dissolution) origins
315 and are found as grain coats or pore-filling matrices. The illite grain coats in Elgin Field are also found
316 coating authigenic quartz, and the matrices are frequently impregnated with bitumen (Fig. 7).
317 Partially or completely dissolved feldspars, with their initial shape preserved as hollow clay rims, are
318 common features in the Elgin field, but infrequently observed in Clyde Field. Intragranular porosity,
319 which is the measure of dissolved feldspars in the analysed thin sections, averages 0.9% in Clyde and
320 3.3% in Elgin (Fig. 7E and F; Table 2). Intragranular porosity from feldspar dissolution was probably
321 underestimated in Clyde samples, as oversized intergranular pore spaces which are most likely sites
322 of dissolved grains are present in the samples. Carbonate cements are around 9% in the Fulmar
323 sandstone samples from both fields (Table 2). These carbonates are often found occluding available
324 pore spaces or destroying porosity locally. Some carbonates were also found as replacive cements in
325 Elgin samples, where they either partially or completely replace dissolved mineral grains.
326 Mineralogically, these carbonate cements occur as discrete dolomite, ferroan dolomite, and as

327 ferroan dolomites surrounding dolomite cores. In addition to dolomite and ferroan dolomites,
328 syntaxial ankerite rims on dolomite nuclei were commonly observed in Elgin samples. Lithic
329 fragments, micas and pyrite are the other minor components common to samples from both fields,
330 with glauconite observed only in Clyde.

331 **4.2.1 Quartz Cementation**

332 Two types of quartz cements, macroquartz and microquartz, were observed by qualitative
333 petrographic analysis (Fig. 7, Fig. 8, and Fig. 9). The macroquartz cements occur as syntaxial and
334 blocky overgrowths and are optically continuous with their detrital quartz nuclei under transmitted
335 light. Different cathodoluminescence zoning patterns can be observed within some of the
336 macroquartz overgrowths at high resolution (Fig. 8). In contrast, microquartz overgrowths are thin,
337 randomly oriented, polycrystalline quartz overgrowths, with lengths usually ranging from 1 to 10 μm
338 (Aase et al., 1996; French and Worden, 2013).

339 Quantitative cathodoluminescence petrographic data from the Central North Sea samples (Table 2)
340 show sandstones from Elgin and Clyde Fields have similar volumes of macroquartz cement (4.6 %
341 and 4.4% respectively). However, normalization of macroquartz cement volume to detrital quartz
342 content, which is required to avoid bias resulting from variations in the detrital mineralogical
343 composition of the samples (see Houseknecht, 1984, 1988, 1991), indicates that Clyde samples have
344 20% more macroquartz cement than Elgin samples (Table 2).

345 For the Gulf of Mexico Wilcox Group, the sample from Lake Creek Field has macroquartz cement
346 content of 18.8 % compared with 12.3 % in the higher temperature Rotherwood samples. Although
347 this study only investigated two samples from the Wilcox Group sandstones, the high volume of
348 quartz cement measured in this study is comparable to the average 12 volume % measured by
349 (Grigsby et al., 1992) from forty-six Wilcox Group sandstones from Lake Creek Field. After
350 normalisation to detrital quartz content, the Lake Creek sample has 37 % more macroquartz cement

351 than the sample from Rotherwood Field (Table 3). The studied Wilcox samples have at least 40 %
352 more macroquartz cement than the Fulmar Formation samples at equivalent temperatures.

353 In all cases, observed macroquartz cement volumes in these Fulmar Formation and Wilcox Group
354 sandstones are lower than those predicted by the quartz cementation model (Table 4; Fig. 11).
355 Modelled quartz cement volumes can always be matched to observed volumes by changing the
356 precipitation kinetic constants a and b in equation 2. However, very different values of a and b are
357 needed in each of the four cases, implying that cementation is not a unique function of temperature.
358 The same conclusion would be drawn if Arrhenius-based kinetics were used to model quartz cement;
359 it would be possible to alter the pre-exponential factor and activation energies within the equation
360 to obtain a local calibration to the amount of quartz cement, but very different constants would be
361 needed to model the quartz cement volumes in the North Sea sandstones compared to the Gulf of
362 Mexico sandstones. Given the relative simplicity of the quartz precipitation reaction, one might
363 expect the kinetic constants to be similar in all situations.

364 Microquartz was frequently observed within certain intervals in the Clyde samples where they occur
365 as well developed, and sometimes pore-occluding overgrowths, but are almost absent in Elgin
366 samples (Fig. 7 and Fig. 9). No microquartz was observed in the Wilcox sandstones, as in previous
367 studies (e.g. Dutton and Loucks, 2010; Grigsby et al., 1992; McBride et al., 1991) .

368 4.2.2 Intergranular Pressure Dissolution

369 Estimation of intergranular pressure dissolution along grain contacts was performed on
370 cathodoluminescence images using Sibley and Blatt's (1976) and Houseknecht's (1991) approach
371 (Fig. 6D and 8A). Grain boundaries were projected along grain contacts where dissolution has taken
372 place (Fig. 6D and 8A), and the inferred features were point-counted as percentage volumes of silica
373 dissolved by intergranular pressure dissolution. Quantitative results suggest that the average volume
374 of silica released by intergranular pressure dissolution is 2.7 % in Clyde, 2.7 % in Elgin, 11.7 % in
375 Rotherwood and 19.7 % in Lake Creek (Tables 2 and 3). Normalization of grain loss to detrital quartz
376 content (see Houseknecht, 1984, 1988, 1991) (shows that approximately 20 % more silica is released
377 by intergranular pressure dissolution in the Fulmar Formation samples from Clyde Field than in
378 higher temperature, low vertical effective stress samples from Elgin Field (Table 2). Similar
379 observations were made for the Wilcox Group samples, where approximately 40 % more silica is
380 released by intergranular pressure dissolution in the sandstone samples from Lake Creek Field than
381 in the higher temperature, lower vertical effective stress sample from Rotherwood Field (Table 3).
382 Inter-basinal comparison of the normalised data also shows that at equivalent temperatures, > 45 %
383 more silica is released by intergranular pressure dissolution in the studied Wilcox Group sandstones
384 than their Fulmar Formation counterparts.

385 In summary, while accepting that this is a small set of sandstones, the combined results from the
386 four fields (Table 5; Figure 5; Figure 12) suggest that:

- 387 a) There is a strong positive relationship between the extent of intergranular pressure
388 dissolution and the amount of quartz cement. Most of the quartz cement can be supplied via
389 intergranular pressure dissolution, with additional silica from feldspar dissolution.
- 390 b) At a given temperature, when normalised to detrital quartz, there is much more quartz
391 cement in the Wilcox sandstones than the Fulmar sandstones.
- 392 c) The Fulmar sandstones in this study have been subjected to much lower effective stresses
393 through most of their history, compared to the Wilcox sandstones.

394

395 4.2.3 Oxygen Isotope Composition of Macroquartz Cements

396 High resolution SIMS analysis has proven to be a valuable tool for reconstructing cementation
397 histories of diagenetic quartz cement, by measuring $\delta^{18}\text{O}$ profiles across individual macroquartz
398 overgrowths (e.g. Harwood et al., 2013; Pollington et al., 2011).

399 Seventy-two $\delta^{18}\text{O}$ measurements were made on six different overgrowths from two sandstones
400 from Clyde and Elgin sample sets. All $\delta^{18}\text{O}_{(\text{qc})}$ results are shown as a function of the distance from
401 their detrital grain boundary in (Fig. 10). Values of $\delta^{18}\text{O}_{(\text{qc})}$ in the Fulmar sandstone sample from
402 Clyde shows a 4.1‰ range from +26.8 to +22.7 ‰, while results from the Elgin sample fall within a
403 2.7 ‰ range, from +22.4 to +19.7 ‰ (Fig. 10).

404 Seventy-nine $\delta^{18}\text{O}$ measurements were also made by ion microprobe on ten different overgrowths
405 from two Wilcox sandstone samples from Lake Creek and Rotherwood Fields (Harwood, 2011). The
406 $\delta^{18}\text{O}_{(\text{qc})}$ of analysed overgrowths in the Wilcox samples show a 6.1‰ range from +24.7 to +18.6 ‰
407 for the Lake Creek sample, and a 5.5‰ range from +23.8 to +18.3 ‰ for the Rotherwood sample.

408 Analyses compromised by the occurrence of fluid inclusions or which fell within cracks or included
409 detrital quartz were discarded. Apart from Elgin, where $\delta^{18}\text{O}_{(\text{qc})}$ does not change across the
410 overgrowths, $\delta^{18}\text{O}_{(\text{qc})}$ values for all sandstones decrease from heavier values in the earliest formed
411 cement to lighter values in latest formed cement (Fig. 10). Also, the $\delta^{18}\text{O}_{(\text{qc})}$ versus distance plots (Fig.
412 10) do not show smooth trends from the detrital boundary to the edge of the overgrowth. These
413 fluctuations, combined with the varied CL zoning in overgrowths (e.g. Fig. 8), demonstrates that the
414 development of quartz cements is more complex than a simple concentric growth pattern.

415

416 4.3 Temperature-controlled Quartz Cementation Models

417 Results of the quartz cementation modelling are shown in Figure 11 and predict that, with the
418 exception of Clyde, all the sandstones in this study have experienced sufficient levels of thermal

419 stresses to be completely cemented with quartz. However, there is a very poor agreement between
420 modelled and measured quartz cement volumes (Table 4). The respective 30 and 50% grain-coatings
421 coverage estimated from petrographic analyses for the Fulmar Formation samples from Elgin and
422 Clyde Fields were incorporated in the models. Zero grain-coatings coverage was used for the Wilcox
423 Group sandstones from Rotherwood and Lake Creek Fields. The model overpredicts quartz cement
424 volumes by 50 and 80 % in sandstones from the high temperature Rotherwood and Elgin Fields
425 respectively (Fig. 11 and Table 4). Similarly, the model overpredicts quartz cement volumes by 30
426 and 55 % for the sandstones from Lake Creek and Clyde Fields respectively (Fig. 11 and Table 4).

427

428 5 DISCUSSION

429 5.1 Quartz Cementation Histories

430 Since the oxygen isotope composition of a mineral is a dual function of temperature and $\delta^{18}\text{O}_{(\text{water})}$
431 (Clayton et al., 1972), our $\delta^{18}\text{O}_{(\text{qc})}$ data cannot alone provide a unique temperature history of quartz
432 precipitation. The data can, however, be interpreted to make the most geologically realistic
433 deductions if we make reasonable assumptions about the evolving oxygen isotope composition of
434 the water from which the quartz precipitated. The framework for this is shown in Figure 13 and is
435 based on the quartz-water oxygen isotope fractionation factors reported by Matsuhisa et al. (1979).

436 Present-day $\delta^{18}\text{O}_{(\text{water})}$ in Fulmar Formation sandstones in the Clyde-Elgin area is around +4.5 ‰
437 (Hendry et al., 2000), and values more positive than this are unusual for Jurassic reservoirs in the
438 Central North Sea (Warren et al., 1994). The first quartz cement to precipitate in Clyde sandstones
439 has $\delta^{18}\text{O}_{(\text{qc})}$ of +26.8 ‰, and the first to precipitate in Elgin has $\delta^{18}\text{O}_{(\text{qc})}$ of +22.4 ‰. If precipitation
440 began in waters similar to Jurassic seawater ($\delta^{18}\text{O}_{(\text{water})} = -1$ ‰), this represents 55 °C in Clyde and 80
441 °C in Elgin. Similarly, if the last quartz to form (+22.7 ‰ and +19.7 ‰ in Clyde and Elgin respectively)
442 precipitated from water that had evolved to a value of +4.5 ‰ at present-day, this would

443 correspond to temperatures of 125 °C in Clyde and 150 °C in Elgin (Fig. 13A). The temperature ranges
444 for quartz cementation are then 55-125 °C in Clyde and 80-150 °C in Elgin.

445 A similar logic can be applied to the Wilcox Group sandstones. Here, Land and Fisher (1987)
446 reported present-day $\delta^{18}\text{O}_{(\text{water})}$ ranging from +3.5 to +5.8 ‰ measured over a wide range of
447 temperature for Wilcox Group sandstones from fields adjacent to the study areas (Fig. 13B). If quartz
448 precipitation started with $\delta^{18}\text{O}_{(\text{qc})}$ of +24.7 ‰ in Lake Creek Field and +23.8 ‰ in Rotherwood Field
449 from waters similar to Eocene seawater (-1 ‰), all quartz cementation could have occurred in
450 $\delta^{18}\text{O}_{(\text{water})}$ that evolved from -1 to +3.5 ‰ at the present-day. This would give a temperature window
451 for quartz cementation of 65 to 145 °C in Lake Creek and 74 – 160 °C in Rotherwood Field (Fig. 13B).
452 If $\delta^{18}\text{O}_{(\text{water})}$ in Rotherwood Field is +5.8 ‰, then cementation occurs to maximum burial
453 temperature. These data imply that quartz cementation occurred up to maximum burial
454 temperature only in Lake Creek, and perhaps in Rotherwood Field.

455 It is rather surprising that cementation did not apparently continue to maximum burial temperature.
456 A plausible explanation for is this that cementation did in fact continue up to maximum burial
457 temperature but is not captured by the SIMS data, as it is very difficult to make analyses to the very
458 edge of the quartz overgrowth (Fig. S4). In all cases, however, the amount of cement precipitating
459 within 20-30 °C of the maximum temperatures would be small.

460 The inevitable uncertainties in the interpretation of $\delta^{18}\text{O}_{(\text{qc})}$ data, in terms of the exact range of
461 temperature and thus time over which cementation occurred, means that we cannot determine the
462 precise rate of quartz cementation through the full burial history. In general, the fact that there is
463 much more quartz cement in the younger Wilcox sandstones compared to the older Fulmar
464 sandstones, indicates that cementation rates in the Wilcox sandstones were on average greater than
465 those in the Fulmar sandstones. Similarly, if we assume that quartz cementation started at
466 temperatures between 60 and 80 °C (Walderhaug, 1994a), the Fulmar sandstones have spent much
467 longer in the proposed quartz cementation “window” than the Wilcox sandstones. Placing the

468 $\delta^{18}\text{O}_{(\text{qc})}$ data into the context of the time-temperature and time-vertical effective stress histories (Fig.
469 5) for each well support these qualitative statements and suggests that:

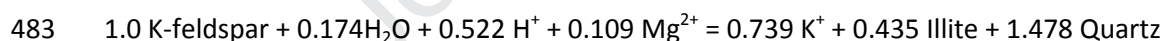
470 a) Quartz cementation rates are on average *slower* in lower vertical effective stress Fulmar
471 Formation sandstones than higher vertical effective stress Wilcox Group sandstones.

472 b) Quartz cementation rates are on average *slower* in Fulmar Formation and Wilcox Group
473 sandstones from the high temperature Elgin and Rotherwood Fields than their low
474 temperature counterparts from Clyde and Lake Creek.

475

476 **5.2 Silica Supply and Quartz Cementation**

477 Quantitative petrographic data show that local, intergranular pressure dissolution could have
478 supplied between 95 - 115 % of the silica required for quartz cementation in the studied Wilcox
479 Group sandstones, and 60% of silica in the studied Fulmar Formation sandstones (Table 5). Fully- or
480 partly-dissolved feldspars occur in both the Fulmar Formation and Wilcox Group sandstones (Fig. 6A
481 and B, Fig. 7E and F) and provide an additional local source of silica via reactions such as the
482 conversion of K-feldspar to illite:



484 Oye et al. (2018) have shown that enough silica is released from this mid-late diagenetic reaction to
485 account for the difference between the observed quartz cement and the silica supplied through
486 intergranular pressure solution in Elgin. Although dissolved feldspar ghosts are less obvious in Clyde
487 compared with Elgin, we suggest that the very common occurrence of oversized pores in Clyde
488 indicates that the silica deficit can be filled in the same way. Fig.12A also suggests that precipitation
489 started around 50°C; an indication that silica for early-formed quartz cement might have been
490 sourced from seawater (Harwood et al., 2013). In summary, in all four cases, all or most of the silica

491 requirement is fulfilled by local intergranular pressure dissolution, with the remainder in the Fulmar
492 sands from local feldspar dissolution.

493

494 **5.3 Does Vertical Effective Stress Exert an Influence on Quartz** 495 **Cementation?**

496 Quantitative petrographic observations, inferred cementation histories, and modelled temperature
497 and vertical effective stress histories combine to suggest that the history of vertical effective stress
498 may exert an important influence on quartz cementation in these four studies. The key observations
499 are:

- 500 1. Although some silica can be sourced from feldspar dissolution in the Fulmar, the majority of
501 the silica required for the observed volumes of quartz cement can be supplied through local
502 intergranular pressure dissolution, in all four case studies (Table 5). The amount and inferred
503 rate of intergranular pressure dissolution is commonly considered to be controlled by
504 vertical effective stress, with a secondary influence of temperature (De Boer et al., 1977;
505 Dewers and Ortoleva, 1990; Dewers and Ortoleva, 1991; Elias and Hajash, 1992; Gratier et
506 al., 2005; Nenna and Aydin, 2011; Oye et al., 2018; Renard et al., 1997; Robin, 1978; Rutter
507 and Elliott, 1976; Sheldon et al., 2003; Shimizu, 1995; Tada et al., 1987; Tada and Siever,
508 1989; van Noort et al., 2008; Weyl, 1959) .
- 509 2. At a given temperature, the amount of quartz cement is much lower in the sandstones that
510 have experienced lower vertical effective stress through their history (Lake Creek versus
511 Clyde; Rotherwood versus Elgin; Fig. 5). In addition, both the Wilcox and Fulmar sandstones
512 buried to higher temperatures and greater thermal stress, Rotherwood and Elgin, have less
513 quartz cement than their lower temperature counterparts (Fig. 11; Table 5).
- 514 3. Measured volumes of quartz cement are lower than those predicted by temperature-
515 controlled precipitation models for all the studied sandstones (Fig. 11 and Fig. 13B),
516 especially for the sandstones that have never experienced high vertical effective stress.

517 Although it would be possible to obtain local calibrations to quartz cement volumes by
518 altering the kinetic constants in either the Walderhaug (1996) or Arrhenius-based (Lander et
519 al., 2008; Taylor et al., 2015; Walderhaug, 2000) quartz cementation models, very different
520 values would be needed for Wilcox and for Fulmar. We suggest that the need for different
521 kinetic constants implies that quartz cementation must be influenced by factors other than
522 the temperature-controlled rate of quartz precipitation (Ajdukiewicz and Lander, 2010;
523 Lander et al., 2008; Walderhaug, 1994a, 1996, 2000).

524 We interpret these observations to suggest that the vertical effective stress-controlled supply of
525 silica from intergranular pressure dissolution exerts an important influence on quartz cementation.
526 This has been suggested previously (Elias and Hajash, 1992; Osborne and Swarbrick, 1999; Oye et al.,
527 2018; Sheldon et al., 2003; van Noort et al., 2008), but the idea may not have gathered support,
528 perhaps because it can be difficult to unravel the relative effects of time-temperature and time-
529 vertical effective stress histories. Accepting that it is difficult to obtain accurate histories of vertical
530 effective stress from basin models, it is not uncommon to observe a general positive relationship
531 between temperature and vertical effective stress during burial. As an illustration, if pore pressure
532 remains hydrostatic throughout the burial history of a sandstone, there will be a very strong
533 correlation between increasing temperature and increasing effective stress through the sediment's
534 burial history. It is only by studying samples from sandstones with very different histories of vertical
535 effective stress, such as those described here, that the relative influence of temperature and stress
536 can be examined.

537 Although beyond the scope of this paper, a critical predictive next step would be to quantify the rate
538 of intergranular pressure dissolution as a dual function of vertical effective stress and temperature.
539 A paper by van Noort et al. (2008) presents such a model, based on higher temperature laboratory
540 experiments, but it has never been tested against data in sandstones in sedimentary basins. Some
541 initial insights can be gleaned from the current study, in that vertical effective stress in Clyde Field

542 has increased from 19 to 40 MPa in the last 0.5 million years but has quartz cement volumes which
543 are qualitatively consistent with the lower vertical effective stress value. This suggests that the
544 kinetics of intergranular pressure dissolution are geologically slow, such that greater (sub million-
545 year) timescales are required for the results of intergranular pressure dissolution to be observed as
546 quartz cement.

547

548 **5.4 Can the pattern of quartz cementation be explained by other factors?**

549 The occurrences of grain-coating clays and microquartz, and the emplacement of petroleum into
550 sandstone reservoirs, have been extensively discussed as ways in which macroquartz cementation
551 can be inhibited. We now discuss - and dismiss - these mechanisms as important controls on quartz
552 cementation in these sandstones.

553 Pervasive grain-coating clays and microquartz are very effective inhibitors of quartz cementation
554 (Ajdukiewicz and Lander, 2010; Berger et al., 2009; Dutton et al., 2016; Morad et al., 2010; Nguyen
555 et al., 2013; Stricker et al., 2016; Taylor et al., 2010; Taylor et al., 2015) but cannot account for the
556 low amounts of cement in these sandstones. In the Wilcox sandstones, microquartz was not
557 observed and some of the minute grain-coating clays present have been engulfed by quartz cement.
558 Grain-coating microquartz was observed in variable abundance in the Clyde sample set. Although
559 samples with the most grain-coating microquartz overgrowths have the least quartz cement,
560 quantitative CL petrography revealed that other samples with little or no microquartz have very low
561 volumes of quartz cement compared to the volume predicted by the temperature-dependent quartz
562 cementation model (Fig. 11 and Table 3). Grain-coating microquartz is very rare in sandstones from
563 Elgin and thus has no effect on quartz cementation.

564 The Fulmar Formation sandstones in this study are upper shoreface facies with low volumes of illitic
565 clays (< 3%). The detrital or authigenic origin of these clays is not easily discernible as detrital illite
566 can recrystallise as a function of temperature (Wilkinson and Haszeldine, 2011). Grain-coating illite

567 derived from feldspar alteration is unlikely to have inhibited quartz cementation, because quartz
568 cement would have precipitated on free detrital quartz surfaces prior to feldspar dissolution (Oye et
569 al., 2018). Petrographic evidence (Fig. 7) confirms this assertion, as authigenic illite coating the
570 surfaces of some macroquartz overgrowths suggests that macroquartz cementation predates
571 authigenic illite formation. Illite of detrital origin forms early on detrital grains and is likely to possess
572 more inhibitive effect on quartz cementation. However, petrographic observation of the Fulmar
573 Formation sandstones shows that poorly-developed grain coatings have been completely engulfed
574 by quartz cement (Fig. 7).

575 Quantitative analysis shows that the combined average grain-coat coverage of clay and microquartz
576 is less than 50% in the Fulmar Formation samples from Clyde and Elgin Fields (Fig. 14). Quartz
577 cementation modelling performed on the Fulmar Formation sandstones were tested with varying
578 grain-coat coverage values. The outputs suggest that each detrital quartz grain requires grain-coat
579 coverage of around 80% in Clyde Field, and 99% in Elgin Field, to limit the observed average quartz
580 cement volumes in both fields to their current values (4.4 and 4.6%). The required coating coverage
581 is thus much higher than those observed.

582 The possible role of hydrocarbon emplacement as an inhibitor of quartz cementation in sandstone
583 reservoirs has been discussed in many studies (e.g. Aase et al., 1996; Aase and Walderhaug, 2005;
584 Dixon et al., 1989; Emery et al., 1993; Gluyas et al., 1993; Marchand et al., 2000; Marchand et al.,
585 2002; Molenaar et al., 2008; Saigal et al., 1992; Wilkinson and Haszeldine, 2011; Worden et al.,
586 2018a; Worden et al., 2018b; Worden et al., 1998). In this study, basin modelling suggests that all
587 the studied sandstones were charged with hydrocarbons from the Miocene, except for the Elgin
588 reservoir that was charged from the Eocene. These timings are similar to those estimated in previous
589 studies of the Fulmar Formation and Wilcox Group sandstones (Pitman and Rowan, 2012;
590 Rudkiewicz et al., 2000; Stevens and Wallis, 1991). Comparison of the charge histories with
591 modelled and actual cementation histories estimated from oxygen isotope data, indicate that the

592 effect of hydrocarbon emplacement on quartz cementation in the studied sandstones is negligible.
593 Firstly, temperature-based quartz precipitation models predict that substantial quartz cement
594 should have precipitated prior to hydrocarbon emplacement and secondly, quartz cementation
595 histories from *in situ* oxygen isotope analysis suggest that cementation continued beyond the time
596 of hydrocarbon emplacement, potentially to the present-day. These results show no evidence that
597 hydrocarbon emplacement has played a significant role on quartz cementation in the studied
598 sandstones.

599

600 **6 SUMMARY AND CONCLUSIONS**

601 We have presented quantitative petrographic data, high spatial resolution oxygen isotope analyses
602 of quartz cement, basin modelling and a kinetic model for quartz precipitation for two Paleocene-
603 Eocene Wilcox Group sandstones from Texas and two Jurassic Fulmar Formation sandstones from
604 the Central North Sea. In each basin, one sandstone has been buried to *ca.* 145 °C and one to *ca.* 185
605 °C.

606 The amounts of quartz cement in the Wilcox sandstones are between 12 and 18%, and between 2
607 and 6% in the Fulmar sandstones. Oxygen isotope data suggest that in all cases, quartz cementation
608 occurred from 60-80 °C to temperatures close to maximum burial. Petrographic data show that most
609 of the silica for quartz cement can be derived from intergranular pressure dissolution, with an
610 additional contribution in Fulmar sandstones from feldspar alteration. There is no strong evidence
611 that factors such as grain coatings or the timing of petroleum emplacement can explain the
612 differences in the amounts of quartz cement in these Wilcox and Fulmar samples.

613 A key difference between the Wilcox and Fulmar sandstones is their history of vertical effective
614 stress. The Wilcox sandstones in this study are currently at much higher vertical effective stresses
615 than the Fulmar sandstones, and basin modelling studies suggest that they have been subjected to

616 generally higher vertical effective stresses through their burial history. Both the extent of
617 intergranular pressure dissolution and of quartz cementation are more strongly related to vertical
618 effective stress than to temperature. We therefore suggest that the differences in quartz
619 cementation in Fulmar and Wilcox sandstones can be explained better by differences in their vertical
620 effective stress history than their temperature history. In this case, the rate of intergranular pressure
621 solution would be an important control on quartz cementation, and an important next step would
622 be to quantify the rate of intergranular pressure dissolution as a function of both vertical effective
623 stress and temperature. In the Clyde case study presented here, vertical effective stress has
624 increased from 19 to 40 MPa in the last 0.5 million years but sandstones have quartz cement
625 volumes which are qualitatively consistent with the lower vertical effective stress value. This
626 suggests that the kinetics of intergranular pressure dissolution are slow on a sub million-year
627 timescale.

628 Because it is not uncommon for both temperature and vertical effective stress to increase as
629 sedimentary rocks are buried, it can be difficult to unravel the relative importance of temperature
630 and vertical effective stress histories as potential controls on quartz cementation. From a petroleum
631 exploration perspective, the limited datasets presented here suggest that sandstones which have
632 been buried to high temperature but which have been subjected to a history of low effective stress,
633 could still be effective reservoirs.

634

635 **7 ACKNOWLEDGMENTS**

636 Petroleum Technology Development Fund, Nigeria is thanked for funding this research. We
637 acknowledge support from the British Geological Survey (BGS) for access to core material, and
638 Information Handling Services (IHS) for access to data from Central North Sea wells. Core samples of
639 Wilcox sandstones were provided to Joseph Harwood by the Bureau of Economic Geology, The
640 University of Texas at Austin. Some of those samples were used in this study. WiscSIMS is supported

641 by the U.S. National Science Foundation (EAR-1658823) and the University of Wisconsin- Madison.

642 JWV is supported by the U.S. Department of Energy, Office of Basic Energy Sciences, Geosciences

643 under Award Number DE-FG02-93ER14389. We thank anonymous reviewers for their constructive

644 comments on the original manuscript.

645

Journal Pre-proof

646 **8 REFERENCES**

- 647 Aase, N.E., Bjorkum, P.A., Nadeau, P.H., 1996. The effect of grain-coating microquartz on
648 preservation of reservoir porosity. *AAPG bulletin* 80, 1654-1673.
- 649 Aase, N.E., Walderhaug, O., 2005. The effect of hydrocarbons on quartz cementation: diagenesis in
650 the Upper Jurassic sandstones of the Miller Field, North Sea, revisited. *Petroleum Geoscience* 11,
651 215-223.
- 652 Ajdukiewicz, J., Nicholson, P., Esch, W., 2010. Prediction of deep reservoir quality using early
653 diagenetic process models in the Jurassic Norphlet Formation, Gulf of Mexico. *AAPG bulletin* 94,
654 1189-1227.
- 655 Ajdukiewicz, J.M., Lander, R.H., 2010. Sandstone reservoir quality prediction: The state of the art.
656 *AAPG bulletin* 94, 1083-1091.
- 657 Allen, P., Allen, J., 1990. *Basin Analysis—Principles and Applications*, 1st ed. Blackwell Scientific
658 Publications, Oxford, p. 449.
- 659 Berger, A., Gier, S., Krois, P., 2009. Porosity-preserving chlorite cements in shallow-marine
660 volcanoclastic sandstones: Evidence from Cretaceous sandstones of the Sawan gas field, Pakistan.
661 *AAPG bulletin* 93, 595-615.
- 662 Bjorkum, P.A., 1996. How important is pressure in causing dissolution of quartz in sandstones?
663 *Journal of Sedimentary Research* 66, 147-154.
- 664 Bjorlykke, K., Egeberg, P., 1993. Quartz cementation in sedimentary basins. *AAPG bulletin* 77, 1538-
665 1548.
- 666 Bloch, S., Lander, R.H., Bonnell, L., 2002. Anomalously high porosity and permeability in deeply
667 buried sandstone reservoirs: Origin and predictability. *AAPG bulletin* 86, 301-328.
- 668 Clayton, R.N., O'Neil, J.R., Mayeda, T.K., 1972. Oxygen isotope exchange between quartz and water.
669 *Journal of Geophysical Research* 77, 3057-3067.
- 670 De Boer, R., Nagtegaal, P., Duyvis, E., 1977. Pressure solution experiments on quartz sand.
671 *Geochimica et Cosmochimica acta* 41, 257-264.
- 672 Dewers, T., Ortoleva, P., 1990. A coupled reaction/transport/mechanical model for intergranular
673 pressure solution, stylolites, and differential compaction and cementation in clean sandstones.
674 *Geochimica et Cosmochimica Acta* 54, 1609-1625.
- 675 Dewers, T., Ortoleva, P., 1991. Influences of clay minerals on sandstone cementation and pressure
676 solution. *Geology* 19, 1045-1048.
- 677 Dixon, S., Summers, D., Surdam, R., 1989. Diagenesis and preservation of porosity in Norphlet
678 Formation (Upper Jurassic), southern Alabama. *AAPG Bulletin* 73, 707-728.
- 679 Dutton, S.P., Ambrose, W.A., Loucks, R.G., 2016. Diagenetic Controls on Reservoir Quality in Deep
680 Upper Wilcox Sandstones of the Rio Grande Delta System, South Texas. *Gulf Coast Association of
681 Geological Societies* 5, 95-110.
- 682 Dutton, S.P., Loucks, R.G., 2010. Diagenetic controls on evolution of porosity and permeability in
683 lower Tertiary Wilcox sandstones from shallow to ultradeep (200–6700m) burial, Gulf of Mexico
684 Basin, USA. *Marine and Petroleum Geology* 27, 69-81.
- 685 Elias, B.P., Hajash, A., 1992. Changes in quartz solubility and porosity due to effective stress: An
686 experimental investigation of pressure solution. *Geology* 20, 451-454.
- 687 Emery, D., Smalley, P., Oxtoby, N., Ragnarsdottir, K., Aagaard, P., Halliday, A., Coleman, M.,
688 Petrovich, R., 1993. Synchronous oil migration and cementation in sandstone reservoirs
689 demonstrated by quantitative description of diagenesis. *Philosophical Transactions of the Royal
690 Society of London A: Mathematical, Physical and Engineering Sciences* 344, 115-125.
- 691 Fisher, W.L., McGowen, J., 1967. Depositional Systems in the Wilcox Group of Texas and Their
692 Relationship to Occurrence of Oil and Gas *Gulf Coast Association of Geological Societies Transactions*
693 17, 105 - 125.
- 694 French, M.W., Worden, R.H., 2013. Orientation of microcrystalline quartz in the Fontainebleau
695 Formation, Paris Basin and why it preserves porosity. *Sedimentary Geology* 284, 149-158.

- 696 French, M.W., Worden, R.H., Mariani, E., Larese, R.E., Mueller, R.R., Kliewer, C.E., 2012.
697 Microcrystalline quartz generation and the preservation of porosity in sandstones: Evidence from
698 the Upper Cretaceous of the Subhercynian Basin, Germany. *Journal of Sedimentary Research* 82,
699 422-434.
- 700 Galloway, W.E., Ganey-Curry, P.E., Li, X., Buffler, R.T., 2000. Cenozoic depositional history of the Gulf
701 of Mexico basin. *AAPG bulletin* 84, 1743-1774.
- 702 Gilham, R., Hercus, C., Evans, A., De Haas, W., 2005. Shearwater (UK Block 22/30b): managing
703 changing uncertainties through field life, Geological Society, London, Petroleum Geology Conference
704 series. Geological Society of London, pp. 663-673.
- 705 Gluyas, J., Robinson, A., Emery, D., Grant, S., Oxtoby, N., 1993. The link between petroleum
706 emplacement and sandstone cementation, Geological Society, London, Petroleum Geology
707 Conference series. Geological Society of London, pp. 1395-1402.
- 708 Gowland, S., 1996. Facies characteristics and depositional models of highly bioturbated shallow
709 marine siliciclastic strata: an example from the Fulmar Formation (Late Jurassic), UK Central Graben.
710 Geological Society, London, Special Publications 114, 185-214.
- 711 Gratier, J.-P., Muquet, L., Hassani, R., Renard, F., 2005. Experimental microstylolites in quartz and
712 modeled application to natural stylolitic structures. *Journal of Structural Geology* 27, 89-100.
- 713 Grigsby, J.D., Vidal, J.M., Luffel, D.L., Hawkins, J., Mendenhall, J.M., 1992. Effects of fibrous illite on
714 permeability measurements from preserved cores obtained in lower Wilcox Group gas sandstones,
715 Lake Creek Field, Montgomery County, Texas. *Gulf Coast Association of Geological Societies*
716 *Transactions* 42, 161-172.
- 717 Harwood, J., 2011. The origin and timing of quartz cementation in reservoir sandstones: evidence
718 from in-situ microanalysis of oxygen isotopes, Geosciences. Newcastle University, Newcastle
719 University, p. 310.
- 720 Harwood, J., Aplin, A.C., Fialips, C.I., Iliffe, J.E., Kozdon, R., Ushikubo, T., Valley, J.W., 2013. Quartz
721 Cementation History of Sandstones Revealed By High-Resolution Sims Oxygen Isotope Analysis.
722 *Journal of Sedimentary Research* 83, 522-530.
- 723 Heald, M., Larese, R., 1974. Influence of coatings on quartz cementation. *Journal of Sedimentary*
724 *Research* 44, 1269-1274.
- 725 Hendry, J.P., Wilkinson, M., Fallick, A.E., Haszeldine, R.S., 2000. Ankerite cementation in deeply
726 buried Jurassic sandstone reservoirs of the central North Sea. *Journal of Sedimentary Research* 70,
727 227-239.
- 728 Houseknecht, D.W., 1984. Influence of grain size and temperature on intergranular pressure
729 solution, quartz cementation, and porosity in a quartzose sandstone. *Journal of Sedimentary*
730 *Research* 54, 348-361.
- 731 Houseknecht, D.W., 1988. Intergranular pressure solution in four quartzose sandstones. *Journal of*
732 *Sedimentary Research* 58, 228-246.
- 733 Houseknecht, D.W., 1991. Use of cathodoluminescence petrography for understanding compaction,
734 quartz cementation, and porosity in sandstones. *SEPM Special Publication SC25*, 59-66.
- 735 Kelly, J.L., Fu, B., Kita, N.T., Valley, J.W., 2007. Optically continuous silcrete quartz cements of the St.
736 Peter Sandstone: high precision oxygen isotope analysis by ion microprobe. *Geochimica et*
737 *Cosmochimica Acta* 71, 3812-3832.
- 738 Kita, N.T., Ushikubo, T., Fu, B., Valley, J.W., 2009. High precision SIMS oxygen isotope analysis and
739 the effect of sample topography. *Chemical Geology* 264, 43-57.
- 740 Kuhn, O., Smith, S., Van Noort, K., Loiseau, B., 2003. The Fulmar Field, Blocks 30/16, 30/11b, UK
741 North Sea. Geological Society, London, *Memoirs* 20, 563-585.
- 742 Land, L.S., Fisher, R.S., 1987. Wilcox sandstone diagenesis, Texas Gulf Coast: a regional isotopic
743 comparison with the Frio Formation. Geological Society, London, *Special Publications* 36, 219-235.
- 744 Lander, R.H., Larese, R.E., Bonnell, L.M., 2008. Toward more accurate quartz cement models: The
745 importance of euhedral versus noneuhedral growth rates. *AAPG Bulletin* 92, 1537-1563.

- 746 Lander, R.H., Walderhaug, O., 1999. Predicting porosity through simulating sandstone compaction
747 and quartz cementation. AAPG bulletin 83, 433-449.
- 748 Lasocki, J., Guemene, J., Hedayati, A., Legorjus, C., Page, W., 1999. The Elgin and Franklin fields: UK
749 Blocks 22/30c, 22/30b and 29/5b, Geological Society, London, Petroleum Geology Conference series.
750 Geological Society of London, pp. 1007-1020.
- 751 Maast, T.E., Jahren, J., Bjorlykke, K., 2011. Diagenetic controls on reservoir quality in Middle to
752 Upper Jurassic sandstones in the South Viking Graben, North Sea. AAPG bulletin 95, 1937-1958.
- 753 Marchand, A., Haszeldine, R., Macaulay, C., Swennen, R., Fallick, A., 2000. Quartz cementation
754 inhibited by crestal oil charge: Miller deep water sandstone, UK North Sea. Clay Minerals 35, 201-
755 201.
- 756 Marchand, A.M., Haszeldine, R.S., Smalley, P.C., Macaulay, C.I., Fallick, A.E., 2001. Evidence for
757 reduced quartz-cementation rates in oil-filled sandstones. Geology 29, 915-918.
- 758 Marchand, A.M., Smalley, P.C., Haszeldine, R.S., Fallick, A.E., 2002. Note on the importance of
759 hydrocarbon fill for reservoir quality prediction in sandstones. AAPG bulletin 86, 1561-1572.
- 760 Matsuhisa, Y., Goldsmith, J.R., Clayton, R.N., 1979. Oxygen isotopic fractionation in the system
761 quartz-albite-anorthite-water. Geochimica et Cosmochimica Acta 43, 1131-1140.
- 762 McBride, E., Diggs, T., Wilson, J., 1991. Compaction of Wilcox and Carrizo sandstones (Paleocene-
763 Eocene) to 4420 M, Texas Gulf Coast. Journal of Sedimentary Research 61, 93 - 85.
- 764 McBride, E.F., 1989. Quartz cement in sandstones: a review. Earth-Science Reviews 26, 69-112.
- 765 Molenaar, N., Cyziene, J., Sliupa, S., Craven, J., 2008. Lack of inhibiting effect of oil emplacement on
766 quartz cementation: Evidence from Cambrian reservoir sandstones, Paleozoic Baltic Basin.
767 Geological society of America bulletin 120, 1280-1295.
- 768 Morad, S., Al-Ramadan, K., Ketzer, J.M., De Ros, L., 2010. The impact of diagenesis on the
769 heterogeneity of sandstone reservoirs: A review of the role of depositional facies and sequence
770 stratigraphy. AAPG bulletin 94, 1267-1309.
- 771 Nenna, F., Aydin, A., 2011. The formation and growth of pressure solution seams in clastic rocks: A
772 field and analytical study. Journal of Structural Geology 33, 633-643.
- 773 Nguyen, B.T., Jones, S.J., Goult, N.R., Middleton, A.J., Grant, N., Ferguson, A., Bowen, L., 2013. The
774 role of fluid pressure and diagenetic cements for porosity preservation in Triassic fluvial reservoirs of
775 the Central Graben, North Sea. AAPG bulletin 97, 1273-1302.
- 776 Nunn, J.A., Sassen, R., 1986. The framework of hydrocarbon generation and migration, Gulf of
777 Mexico continental slope. Gulf Coast Association of Geological Societies Transactions 36, 257-262.
- 778 Osborne, M.J., Swarbrick, R.E., 1999. Diagenesis in North Sea HPHT clastic reservoirs—Consequences
779 for porosity and overpressure prediction. Marine and Petroleum Geology 16, 337-353.
- 780 Oye, O.J., Aplin, A.C., Jones, S.J., Gluyas, J.G., Bowen, L., Orland, I.J., Valley, J.W., 2018. Vertical
781 effective stress as a control on quartz cementation in sandstones. Marine and Petroleum Geology
782 98, 640-652.
- 783 Page, F., Ushikubo, T., Kita, N.T., Riciputi, L., Valley, J.W., 2007. High-precision oxygen isotope
784 analysis of picogram samples reveals 2 μm gradients and slow diffusion in zircon. American
785 Mineralogist 92, 1772-1775.
- 786 Pitman, J.K., Rowan, E.R., 2012. Temperature and petroleum generation history of the Wilcox
787 Formation, Louisiana, Open-File Report. US Geological Survey, Reston, VA, pp. i-51.
- 788 Pittman, E.D., 1972. Diagenesis of quartz in sandstones as revealed by scanning electron microscopy.
789 Journal of Sedimentary Research 42, 507-519.
- 790 Pollington, A.D., Kozdon, R., Valley, J.W., 2011. Evolution of quartz cementation during burial of the
791 Cambrian Mount Simon Sandstone, Illinois Basin: In situ microanalysis of $\delta^{18}\text{O}$. Geology 39, 1119-
792 1122.
- 793 Renard, F., Ortoleva, P., Gratier, J.P., 1997. Pressure solution in sandstones: influence of clays and
794 dependence on temperature and stress. Tectonophysics 280, 257-266.
- 795 Robin, P.-Y.F., 1978. Pressure solution at grain-to-grain contacts. Geochimica et Cosmochimica Acta
796 42, 1383-1389.

- 797 Robinson, A., Gluyas, J., 1992. Model calculations of loss of porosity in sandstones as a result of
798 compaction and quartz cementation. *Marine and Petroleum Geology* 9, 319-323.
- 799 Rudkiewicz, J., Pentead, H.d.B., Vear, A., Vandenbroucke, M., Brigaud, F., Wendebourg, J.,
800 Duppenbecker, S., 2000. Integrated Basin Modeling Helps to Decipher Petroleum Systems.
801 *Petroleum systems of South Atlantic margins Memoir* 73, 27-40.
- 802 Rutter, E., Elliott, D., 1976. The kinetics of rock deformation by pressure solution. *Philosophical*
803 *Transactions of the Royal Society of London A: Mathematical, Physical and Engineering Sciences* 283,
804 203-219.
- 805 Saigal, G.C., Bjorlykke, K., Larter, S., 1992. The Effects of Oil Emplacement on Diagenetic Processes:
806 Examples from the Fulmar Reservoir Sandstones, Central North Sea: *Geologic Note* (1). AAPG
807 *Bulletin* 76, 1024-1033.
- 808 Sathar, S., Worden, R.H., Faulkner, D.R., Smalley, P.C., 2012. The effect of oil saturation on the
809 mechanism of compaction in granular materials: higher oil saturations lead to more grain fracturing
810 and less pressure solution. *Journal of Sedimentary Research* 82, 571-584.
- 811 Sheldon, H.A., Wheeler, J., Worden, R.H., Cheadle, M.J., 2003. An analysis of the roles of stress,
812 temperature, and pH in chemical compaction of sandstones. *Journal of Sedimentary Research* 73,
813 64-71.
- 814 Shimizu, I., 1995. Kinetics of pressure solution creep in quartz: theoretical considerations.
815 *Tectonophysics* 245, 121-134.
- 816 Sibley, D.F., Blatt, H., 1976. Intergranular pressure solution and cementation of the Tuscarora
817 orthoquartzite. *Journal of Sedimentary Research* 46, 881-896.
- 818 Smith, D.L., Dees, W.T., Harrelson, D.W., 1981. Geothermal conditions and their implications for
819 basement tectonics in the Gulf Coast margin. *Gulf Coast Association of Geological Societies*
820 *Transactions* 31, 181-190.
- 821 Stevens, D., Wallis, R., 1991. The Clyde Field, Block 30/17b, UK North Sea. *Geological Society,*
822 *London, Memoirs* 14, 279-285.
- 823 Stricker, S., Jones, S., 2016. Enhanced porosity preservation by pore fluid overpressure and chlorite
824 grain coatings in the Triassic Skagerrak, Central Graben, North Sea, UK. *Geological Society special*
825 *publications*. 435, 321-341.
- 826 Stricker, S., Jones, S.J., Sathar, S., Bowen, L., Oxtoby, N., 2016. Exceptional reservoir quality in HPHT
827 reservoir settings: Examples from the Skagerrak Formation of the Heron Cluster, North Sea, UK.
828 *Marine and Petroleum Geology* 77, 198-215.
- 829 Swarbrick, R., Osborne, M., Grunberger, D., Yardley, G., Macleod, G., Aplin, A., Larter, S., Knight, I.,
830 Auld, H., 2000. Integrated study of the Judy Field (Block 30/7a)—an overpressured Central North Sea
831 oil/gas field. *Marine and Petroleum Geology* 17, 993-1010.
- 832 Swarbrick, R., Seldon, B., Mallon, A., 2005. Modelling the Central North Sea pressure history.
833 *Geological Society, London, Petroleum Geology Conference series* 6, 1237-1245.
- 834 Swarbrick, R.E., Lahann, R.W., O'Connor, S.A., Mallon, A.J., 2010. Role of the Chalk in development of
835 deep overpressure in the Central North Sea. *Geological Society, London, Petroleum Geology*
836 *Conference series* 7, 493-507.
- 837 Tada, R., Maliva, R., Siever, R., 1987. A new mechanism for pressure solution in porous quartzose
838 sandstone. *Geochimica et Cosmochimica Acta* 51, 2295-2301.
- 839 Tada, R., Siever, R., 1989. Pressure Solution During Diagenesis. *Annual Review of Earth and Planetary*
840 *Sciences* 17, 89-118.
- 841 Taylor, T.R., Giles, M.R., Hathon, L.A., Diggs, T.N., Braunsdorf, N.R., Birbiglia, G.V., Kittridge, M.G.,
842 Macaulay, C.I., Espejo, I.S., 2010. Sandstone diagenesis and reservoir quality prediction: Models,
843 myths, and reality. *AAPG bulletin* 94, 1093-1132.
- 844 Taylor, T.R., Kittridge, M.G., Winefield, P., Bryndzia, L.T., Bonnell, L.M., 2015. Reservoir quality and
845 rock properties modeling—Triassic and Jurassic sandstones, greater Shearwater area, UK Central
846 North Sea. *Marine and Petroleum Geology* 65, 1-21.

- 847 Terzaghi, K., 1925. Principles of soil mechanics, IV—Settlement and consolidation of clay.
848 Engineering News-Record 95, 874-878.
- 849 Valley, J.W., Kita, N.T., 2009. In situ oxygen isotope geochemistry by ion microprobe. MAC short
850 course: secondary ion mass spectrometry in the earth sciences 41, 19-63.
- 851 van Noort, R., Spiers, C.J., Pennock, G.M., 2008. Compaction of granular quartz under hydrothermal
852 conditions: Controlling mechanisms and grain boundary processes. *Journal of Geophysical Research:*
853 *Solid Earth* 113, 1-23.
- 854 Walderhaug, O., 1994a. Temperatures of quartz cementation in Jurassic sandstones from the
855 Norwegian continental shelf—evidence from fluid inclusions. *Journal of Sedimentary Research* 64,
856 311-323.
- 857 Walderhaug, O., 1994b. Precipitation rates for quartz cement in sandstones determined by fluid-
858 inclusion microthermometry and temperature-history modeling. *Journal of Sedimentary Research*
859 64, 324-333.
- 860 Walderhaug, O., 1996. Kinetic modeling of quartz cementation and porosity loss in deeply buried
861 sandstone reservoirs. *AAPG bulletin* 80, 731-745.
- 862 Walderhaug, O., 2000. Modeling quartz cementation and porosity in Middle Jurassic Brent Group
863 sandstones of the Kvitebjørn field, northern North Sea. *AAPG bulletin* 84, 1325-1339.
- 864 Walderhaug, O., Lander, R., Bjørkum, P., Oelkers, E., Bjørlykke, K., Nadeau, P., 2000. Modelling
865 quartz cementation and porosity in reservoir sandstones: examples from the Norwegian continental
866 shelf, in: Worden, R., Morad, S. (Eds.), *Quartz cementation in sandstones*, Special Publication
867 International Association of Sedimentologists, v. 29, pp. 39 - 49.
- 868 Waldschmidt, W.A., 1941. Cementing materials in sandstones and their probable influence on
869 migration and accumulation of oil and gas. *AAPG Bulletin* 25, 1839-1879.
- 870 Warren, E., Smalley, P., Howarth, R., 1994. Compositional variations of North Sea formation waters.
871 *North Sea formation waters atlas*, 119-140.
- 872 Weyl, P.K., 1959. Pressure solution and the force of crystallization: a phenomenological theory.
873 *Journal of geophysical research* 64, 2001-2025.
- 874 Wilkinson, M., Haszeldine, R.S., 2011. Oil charge preserves exceptional porosity in deeply buried,
875 overpressured, sandstones: Central North Sea, UK. *Journal of the Geological Society* 168, 1285-1295.
- 876 Wilkinson, M., Haszeldine, R.S., Fallick, A.E., 2006. Hydrocarbon filling and leakage history of a deep
877 geopressured sandstone, Fulmar Formation, United Kingdom North Sea. *AAPG bulletin* 90, 1945-
878 1961.
- 879 Worden, R.H., Armitage, P., Butcher, A., Churchill, J., Csoma, A., Hollis, C., Lander, R., Omma, J.,
880 2018a. Petroleum reservoir quality prediction: overview and contrasting approaches from sandstone
881 and carbonate communities. *Geological Society, London, Special Publications* 435, SP435. 421.
- 882 Worden, R.H., Bukar, M., Shell, P., 2018b. The effect of oil emplacement on quartz cementation in a
883 deeply buried sandstone reservoir. *AAPG Bulletin* 102, 49-75.
- 884 Worden, R.H., Morad, S., 2000. Quartz cementation in oil field sandstones: a review of the key
885 controversies. *Quartz cementation in sandstones*, Special publications of international association of
886 sedimentologists 29, 1-20.
- 887 Worden, R.H., Oxtoby, N.H., Smalley, P.C., 1998. Can oil emplacement prevent quartz cementation in
888 sandstones? *Petroleum Geoscience* 4, 129-137.

889

890 Figure 1. Maps of study locations; A) UK Central North Sea (CNS) showing Clyde, Elgin and other
891 surrounding fields: B) Texas showing Lake Creek Field in Montgomery County and the Texaco No. 1
892 Hallson Well, Rotherwood Field in Harris County (Adapted from Fisher and Land (1986) and Day-
893 Stirrat et al. (2010))

894

895 Figure 2. Regional stratigraphy of the Central North Sea from Middle Jurassic to Lower Cretaceous.
896 Shallow marine Fulmar Formation was investigated in this study (adapted from Graham et al. 2003)

897

898 Figure 3. Generalised stratigraphy of the Gulf Coast Tertiary and Quaternary section showing the
899 Paleocene-Eocene Wilcox Group and other formations (adapted from Pitman and Rowan, 2012)

900

901 Figure 4. Burial history reconstruction for the Central North Sea Fulmar Formation sandstones from
902 Clyde and Elgin Fields, and the onshore Gulf of Mexico Wilcox Group sandstones from Rotherwood
903 and Lake Creek Fields. These models were constructed by using a forward modelling approach on
904 PetroMod 1D version 2014.1. Fulmar Formation sandstones are 100Myrs older than the Wilcox
905 Group sandstones. M.J – Middle Jurassic, U.J – Upper Jurassic, Plc – Paleocene, Olig. – Oligocene, P. –
906 Pliocene, TVDSS – True vertical depth subsea.

907

908 Figure 5. Modelled temperature (A) and vertical effective stress (B) histories for Central North Sea
909 Fulmar Formation from Clyde and Elgin fields, and Gulf of Mexico Wilcox sandstones from
910 Rotherwood and Lake Creek. These models were constructed by using a forward modelling approach
911 on PetroMod 1D version 2014.1. Upper Jurassic Fulmar Formation sandstones are 100 Ma older than
912 the Paleocene-Eocene Wilcox Group sandstones. Green dashed line represents the most likely

913 evolution pathway for Fulmar Formation vertical effective stress history in Clyde Field based on
914 Swarbrick et al. (2005) Fulmar Formation sandstones experienced low vertical effective stress (VES)
915 for most of their burial histories compare to Wilcox Group sandstones.

916

917 Figure 6. A) Optical thin-section photomicrograph (plane polarized) of Wilcox sandstone sample from
918 Lake Creek Field showing interlocked mineral grains, pore-filling illite, and grain-coating illite
919 engulfed by quartz cement (QC). Detrital quartz is represented by DQ. B) Optical thin-section
920 photomicrograph (plane polarized) of Wilcox sandstone of Lake Creek Field samples showing
921 secondary porosity from dissolved feldspars. C) Back-scattered electron (BSE) image of Wilcox
922 sandstone sample from Lake Creek Field. The region enclosed in orange circle shows intergranular
923 pressure dissolution. D) Equivalent cathodoluminescence (CL) image of slide C showing example of
924 projected grain boundary (red circle) used for quantification of intergranular pressure dissolution
925 (after Sibley and Blatt (1976) and Houseknecht (1991)). E) Optical thin-section photomicrograph
926 (cross polarized) of Wilcox sandstone sample from Rotherwood Field showing ankerite cement
927 replacing grains (presumably feldspars) in sandstones from Rotherwood Field are visible in cross
928 polarised light image (F). Optical thin-section photomicrograph (cross polarized) of Wilcox sandstone
929 sample from Rotherwood Field showing plagioclase feldspar. Plagioclase feldspars are more
930 common in Wilcox Group sandstones than their Fulmar Formation counterparts.

931

932 Figure 7. A) Cathodoluminescence (CL) image of Fulmar Formation sample from Elgin field showing
933 partially dissolved feldspar, quartz cement and detrital quartz. Quartz overgrowths have stunted
934 growth despite significant porosity and the very high present-day temperature (~190 °C). B) Optical
935 thin-section photomicrograph (plane polarized) of Fulmar Formation sample from Elgin Field
936 showing bitumen impregnated authigenic illite (red arrows) coating already precipitated

937 macroquartz cement surfaces. Macroquartz cements completely engulfed grain-coating illite (black
938 arrow). The blue areas represent porosity (Image from Fig. 6 in Oye et al., 2018). C) Optical thin-
939 section photomicrograph (plane polarized) of Fulmar Formation from Clyde Field showing detrital
940 grains with macroquartz and microquartz overgrowths. Pore-occluding microquartz cements are also
941 present. D) Optical thin-section photomicrograph (plane polarized) of Fulmar Formation from Clyde
942 field showing the coexistence of adjacent detrital grains completely enveloped by either microquartz
943 or macroquartz overgrowths. The orange arrow points to poorly-developed clay coat on the detrital
944 quartz with thick macroquartz overgrowth. The yellow arrow points at the well-developed grain-
945 coating microquartz completely coating available surface area on the other detrital quartz grain. E)
946 Optical thin-section photomicrograph (cross polarized) of Fulmar Formation from Elgin Field showing
947 bitumen-impregnated clay rim preserving the shape of completely dissolved feldspar; the red arrow
948 points at partially dissolved feldspar impregnated with bitumen. F) Optical thin-section
949 photomicrograph (cross polarized) of Fulmar Formation from Clyde field showing altered feldspars,
950 and preserved K-feldspar overgrowth outlining the shape of dissolved detrital K-feldspar.

951

952 Figure 8. Back-scattered electron (BSE) images (left) and equivalent cathodoluminescence (CL)
953 images (right) of Upper Jurassic Fulmar sandstones showing A) sample projected grain boundary
954 (after Sibley and Blatt (1976) and Houseknecht (1991)) used to define and quantify pressure
955 dissolution, and healed grain fractures; B) quartz grain from Clyde sample set with very thick
956 syntaxial overgrowth typified by mosaic-type CL zoning; C) quartz grain from Elgin sample set with
957 syntaxial overgrowth showing angular CL zonation. These zoning patterns show that the idea of a
958 overgrowth nucleating concentrically on detrital quartz, as assumed in quartz cementation model, is
959 not always the case. Generally, overgrowth thicknesses are up to 60 μ m in Elgin samples, and 100 μ m
960 in Clyde samples.

961

962 Figure 9. Micrographs of Upper Jurassic Fulmar Formation sandstones from Clyde and Elgin fields A)
963 Scanning electron microscope (SEM) image of Clyde sample showing macroquartz and microquartz
964 overgrowths nucleated on the same detrital quartz. B) Higher magnification view equivalent to the
965 box in panel A. C) SEM image of Elgin sample showing quartz grain surface with poorly developed
966 microquartz overgrowth and clay coats. D) Higher magnification of the box in panel C. Microquartz
967 overgrowth are effectively absent in the Elgin samples (Images from Fig. 5 in Oye et al., 2018).

968

969 Figure 10. Plot of $\delta^{18}\text{O}_{(\text{quartz cement})}$ against distance in microns from detrital grain boundaries.
970 Distance axis is limited to 50 μm in Elgin, 80 μm in Lake Creek, and 100 μm in Clyde and Rotherwood.
971 Clyde and Elgin data were acquired from three overgrowths each using 3 μm SIMS spot sizes. Lake
972 Creek and Rotherwood data were acquired from six and four overgrowths respectively using 12 μm
973 SIMS spot sizes. All $\delta^{18}\text{O}_{(\text{quartz cement})}$ decrease from heavier values close to detrital grain boundary to
974 lighter values at the outermost edge of the overgrowths with the exception of Elgin samples.

975

976 Figure 11. Models showing quartz precipitation from quartz cementation threshold (80°C) to
977 present-day for Fulmar Formation from Elgin and Clyde Fields, and Wilcox Group sandstones from
978 Rotherwood and Lake Creek Fields. Walderhaug's (1996) approach was applied to 1 cm^3 volume of
979 the studied sandstones using an 80°C threshold temperature for cementation and a starting porosity
980 of 26%. Time-temperature history was generated using PetroMod version 2014.1. Average grain-
981 coatings coverage in Elgin and Clyde samples sets are approximately 30 and 50% respectively. Grain
982 coatings in Clyde Field include both clays and microquartz. Grain coatings are very rare in the studied
983 Wilcox Group sandstones.

984

985 Figure 12. (A) Intergranular pressure dissolution versus quartz cement. All data have been
986 normalized to detrital quartz content to avoid bias that may result from variations in the detrital
987 mineralogical composition of the samples (see Houseknecht 1984; Houseknecht 1988; Houseknecht
988 1991). (B) Measured quartz cement against modelled quartz cement from Walderhaug's (1996)
989 model. Note the low volumes of measured quartz cement compared to modelled quartz cement. (C)
990 Present-day vertical effective stress versus measured quartz cement. (D) Present-day temperature
991 versus measured quartz cement. Each point represents data from a single field. See Table 5 for data
992 plotted in this figure.

993

994 Figure 13. Plot showing $\delta^{18}\text{O}_{(\text{water})}$ in equilibrium with $\delta^{18}\text{O}_{(\text{quartz cement})}$ as a function of temperature
995 (Matsuhisa et al. 1979). (A) Red and black $\delta^{18}\text{O}_{(\text{quartz cement})}$ Vienna Standard Mean Ocean Water
996 (VSMOW) contours represent the $\delta^{18}\text{O}$ range from early to late quartz cement in Clyde and Elgin.
997 $\delta^{18}\text{O}_{(\text{water})}$ likely evolved from Jurassic marine water to present-day formation water (~ 4.5 ‰) in the
998 Fulmar reservoirs in Clyde and Elgin fields. (B) Red and black $\delta^{18}\text{O}_{(\text{quartz cement})}$ VSMOW contours
999 represent $\delta^{18}\text{O}$ range from early to late quartz cement in Lake Creek and Rotherwood Fields.
1000 $\delta^{18}\text{O}_{(\text{water})}$ likely evolved from Tertiary marine water to present-day formation water (+3.5 to + 5.8
1001 ‰) in Lake Creek and in Rotherwood. These $\delta^{18}\text{O}_{(\text{water})}$ are based on measured data from Wilcox
1002 Group sandstones from adjacent fields in the onshore Gulf Coast region (Land and Fisher 1987).
1003 Evolution paths in graphs A and B are depicted by red (Clyde and Lake Creek) and black (Elgin and
1004 Rotherwood) arrows.

1005

1006 Figure 14. Percentage of detrital quartz fraction in the analysed Upper Jurassic Fulmar Formation
1007 sandstones from Clyde and Elgin fields, and their corresponding percentage grain coat coverage.

1008 Average grain coat coverage in both Clyde and Elgin field is less than 40%. The analysed grain
1009 coatings in Clyde include clays and microquartz.

1010

1011

Journal Pre-proof

Table 1. Depth, Vertical Effective Stress and Temperature matrix for the studied Fulmar Formation and Wilcox Group sandstones

Field	Basin	Group/ Formation	Age	Depth (m ssTVD)	Temp (°C)	VES (MPa)
Clyde	UK Central North Sea	Fulmar	Upper Jurassic	3770-3790	147	40.0
Elgin	UK Central North Sea	Fulmar	Upper Jurassic	5410-5435	189	12.3
Lake Creek	Gulf of Mexico	Wilcox	Early Eocene	3518	143	33.4
Rotherwood	Gulf of Mexico	Wilcox	Paleocene- Eocene	5063	185	23.9

Table 2. Petrographic data of the Upper Jurassic Fulmar Formation sandstones from Clyde and Elgin fields, Central North Sea. Number of analysed samples is the same for the two fields. More detailed data are reported in the supplementary material (Fig. S3, Tables S4, S5, S6 and S7)

	Number of samples	Clyde				Elgin			
		Clyde Mean	Clyde Standard Deviation	Clyde Minimum	Clyde Maximum	Elgin Mean	Elgin Standard Deviation	Elgin Minimum	Elgin Maximum
Detrital grain size (mm)	10	0.18	0.06	0.06	0.41	0.16	0.05	0.06	0.36
Quartz (%)	19	38.1	3.9	30.3	44.3	44.2	5.6	32.3	55.7
Feldspar (%)	19	27.3	3.3	19.7	32.7	23.5	3.4	17.3	29.7
Lithic Fragments (%)	19	1.2	0.5	0.0	2.3	1.1	0.7	0.0	2.7
Quartz cement - standard petrography (%)	19	3.6	1.6	0.7	7.0	2.0	1.4	0.3	6.3
Quartz cement - CL petrography (%)	10	4.4	1.1	2.7	5.9	4.6	1.2	2.1	6.4
Intergranular Pressure Dissolution - CL petrography (%)	10	2.7	1.0	1.1	3.8	2.7	0.8	1.4	3.8
Quartz cement normalised to detrital quartz	10	0.15	0.03	0.10	0.20	0.12	0.03	0.05	0.15
Intergranular Pressure Dissolution normalised to detrital quartz	10	0.09	0.03	0.04	0.13	0.07	0.02	0.04	0.10
Carbonate cement (%)	19	8.7	5.1	1.3	21	9.4	12.3	0.0	40
Intergranular porosity (%)	19	12.9	2.7	7.3	17.0	11.0	4.6	1.7	20.7
Intragranular porosity (%)	19	0.9	1.0	0.0	3.0	3.3	1.5	1.0	8.0
Core Porosity (%)	33	24.4	2.1	17.2	29.4	22.0	5.2	8.5	27.9
Authigenic and detrital clay (%)	19	2.3	1.4	0.3	5.3	2.8	2.3	0.7	9.3

Table 3. Petrographic data of the studied Wilcox Group sandstones. All data from Harwood (2011), except Intergranular Pressure Dissolution (IPD) data. Bt = Berthierine, M/I = Mica/Illite, K-F = K-Feldspar, Na-F = Na-Feldspar, Ch = Chlorite, An = Ankerite.

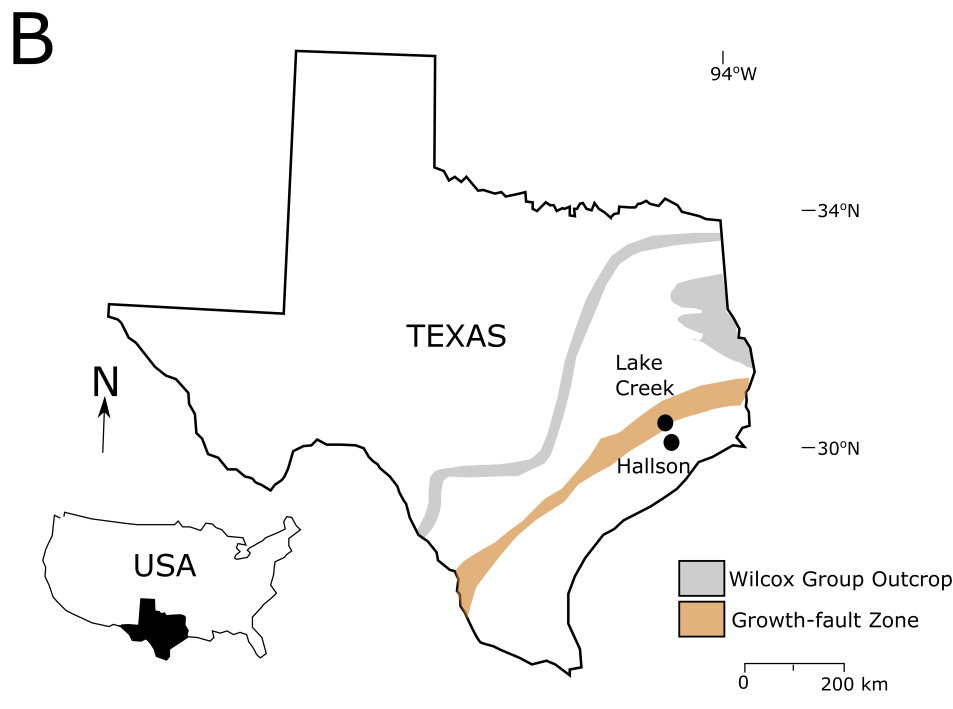
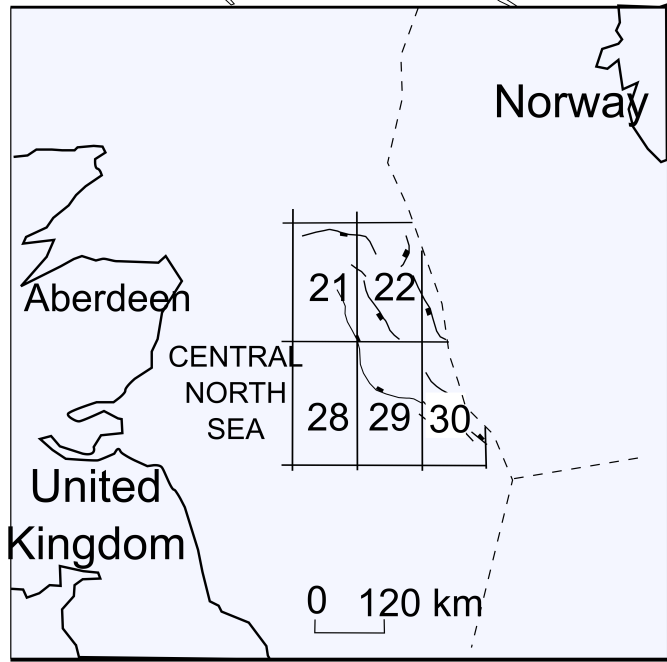
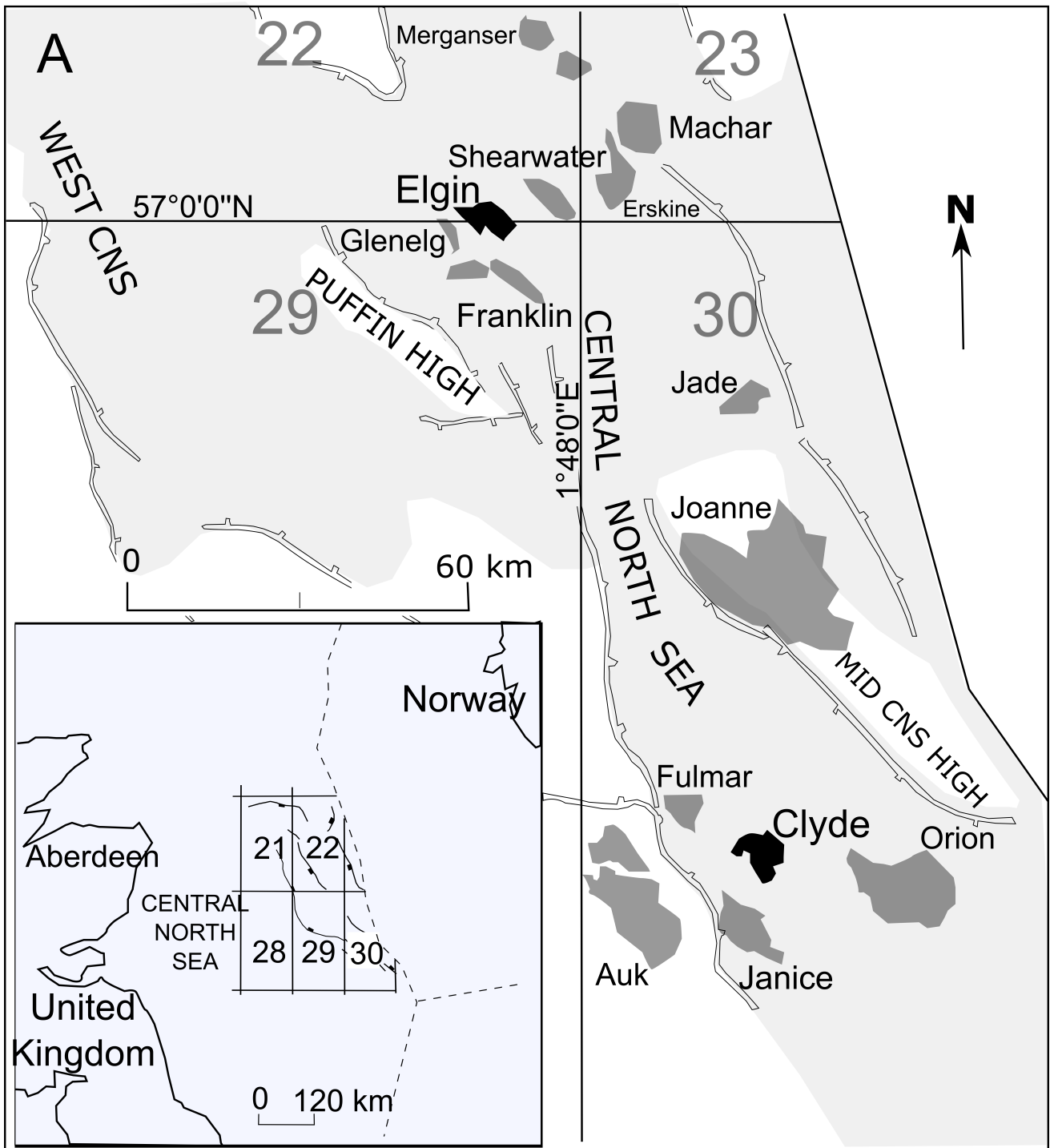
Field	Sample size	Average quartz cement (%)	Average detrital quartz (%)	Quartz Cement /Detrital Quartz	IPD (%)	IPD/Detrital Quartz	Non-quartz minerals (%)	Porosity (%)	Average grain size (mm)
Lake Creek	1	18.8	53.4	0.35	19.7	0.37	M/I, Bt, K-F (16%)	11.8	0.17
Rotherwood	1	12.3	56.9	0.22	11.7	0.21	Ch, M/I, Bt, Na-F, An (24%)	6.8	0.16

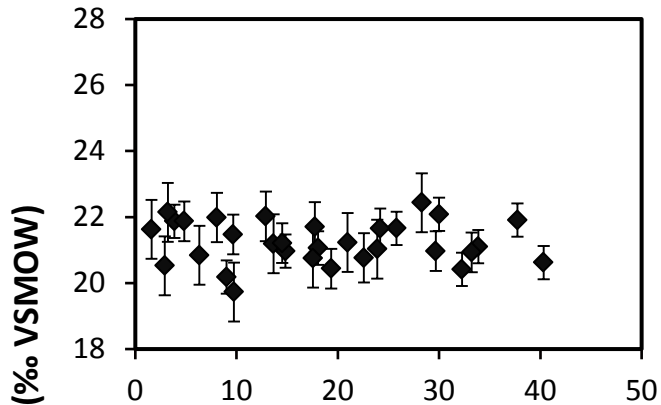
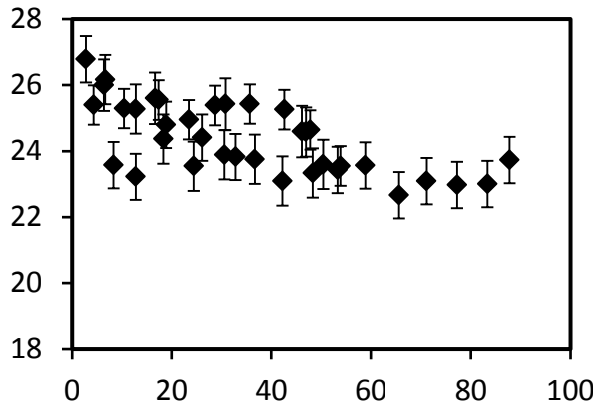
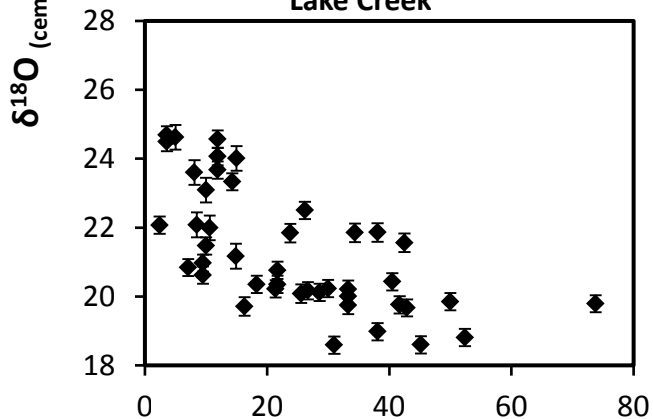
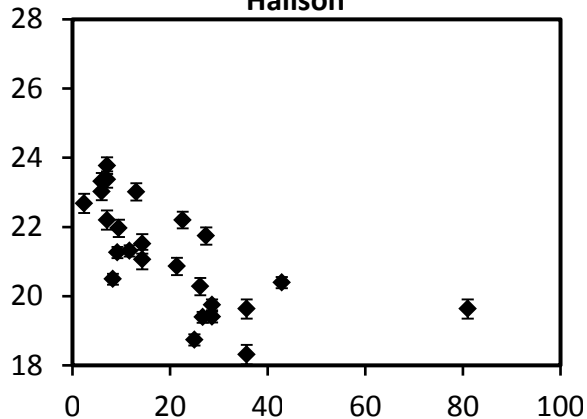
Table 4. Comparison of modelled and measured quartz cement volumes for sandstones from all the study locations

	Clyde	Elgin	Rotherwood	Lake Creek
Temperature (°C)	147	189	185	143
Modelled Quartz Cement (%)	10.1	26.0	26.0	26.0
Measured Quartz Cement (%)	4.4	4.6	12.3	18.8

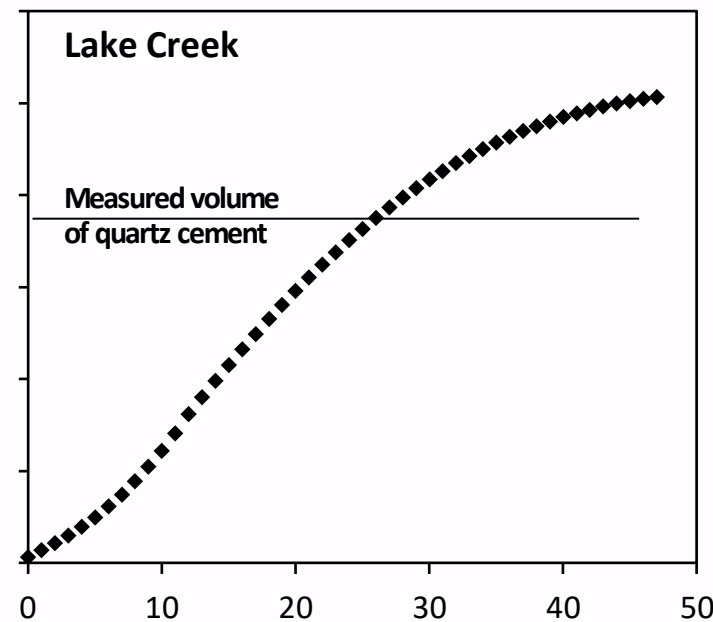
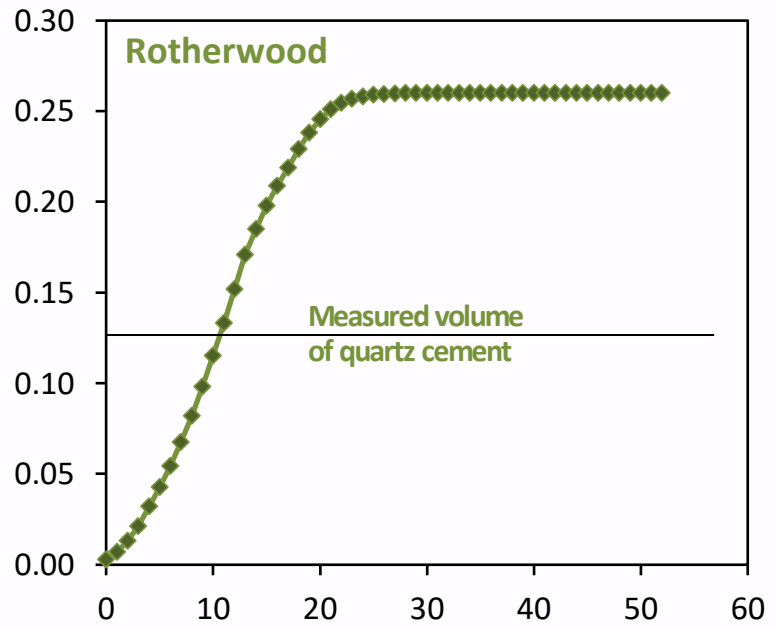
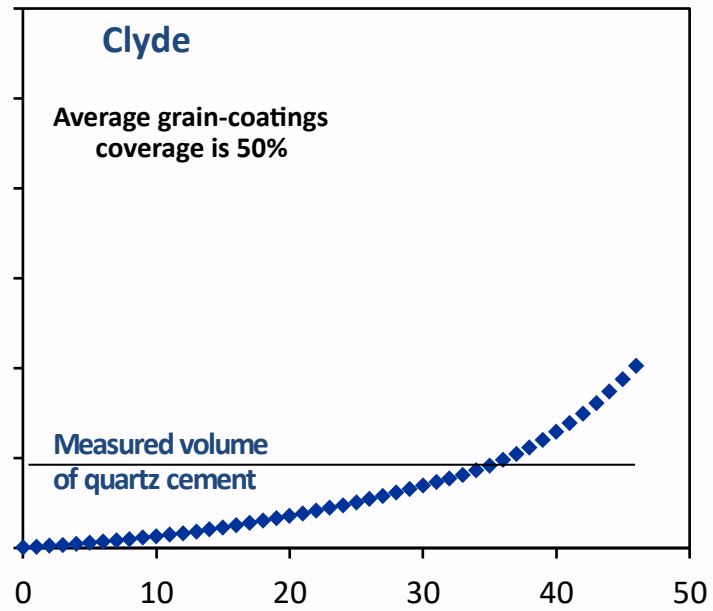
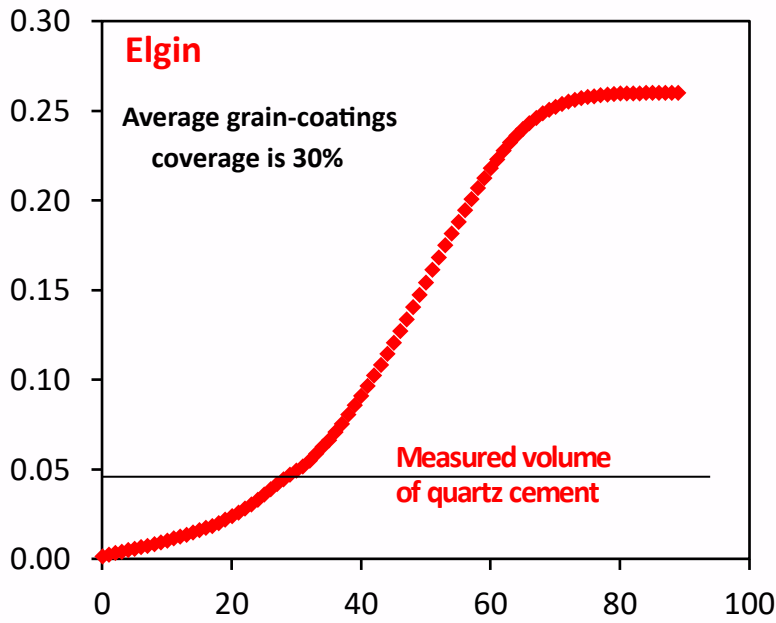
Table 5. Normalized quartz cement contents for the Fulmar Formation and Wilcox Group sandstones. VES = Vertical Effective Stress; $\delta^{18}\text{O}_{(\text{qc})}$ is the oxygen isotope composition of quartz cement. VES in Clyde is the proposed VES 0.5 Ma ago, prior to reduction in pore pressure as a result of lateral fluid drainage (Swarbrick et al., 2005). Present-day VES in Clyde is 40 MPa. Temp. Range is the temperature range over which quartz cement is suggested to form, based on oxygen isotope composition. IPD is intergranular pressure dissolution.

Field	Modelled Quartz Cement (%)	Measured Quartz Cement (%)	Quartz Cement/ Detrital Quartz	IPD/ Detrital Quartz	Temp. (°C)	VES (MPa)	$\delta^{18}\text{O}_{(\text{qc})}$ range	Temp. Range (°C)
Elgin	26.0	4.6	0.12	0.07	189	12.5	2.7	80-150
Clyde	10.1	4.4	0.15	0.09	147	19.2	4.1	55-125
Rotherwood	26.0	12.3	0.22	0.21	185	23.2	5.5	75-160
Lake Creek	26.0	18.8	0.35	0.37	143	33.7	6.1	65-145



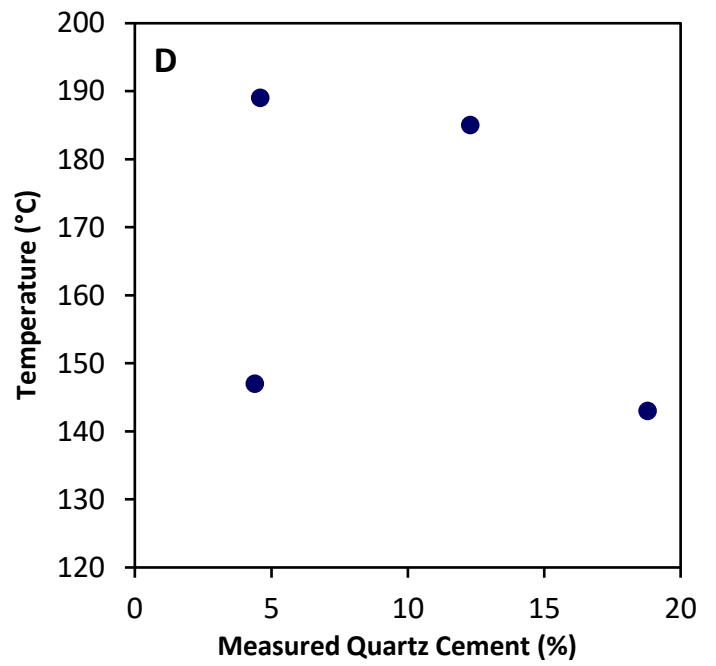
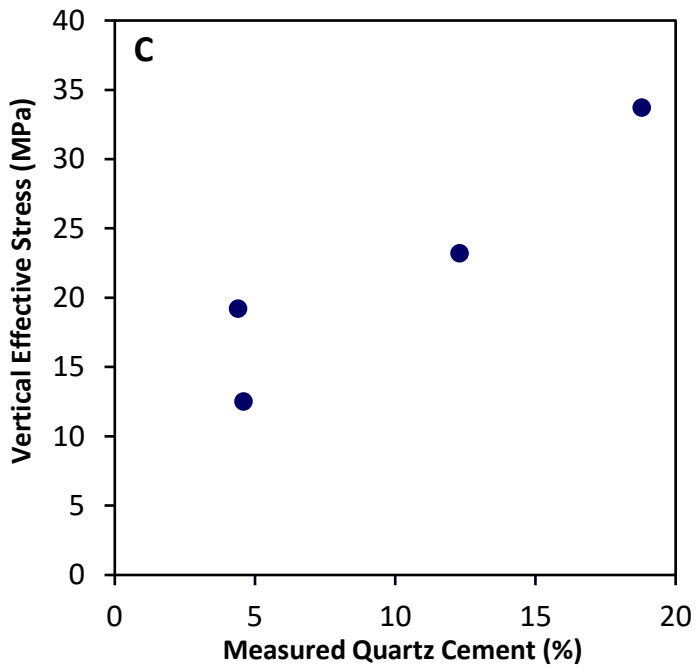
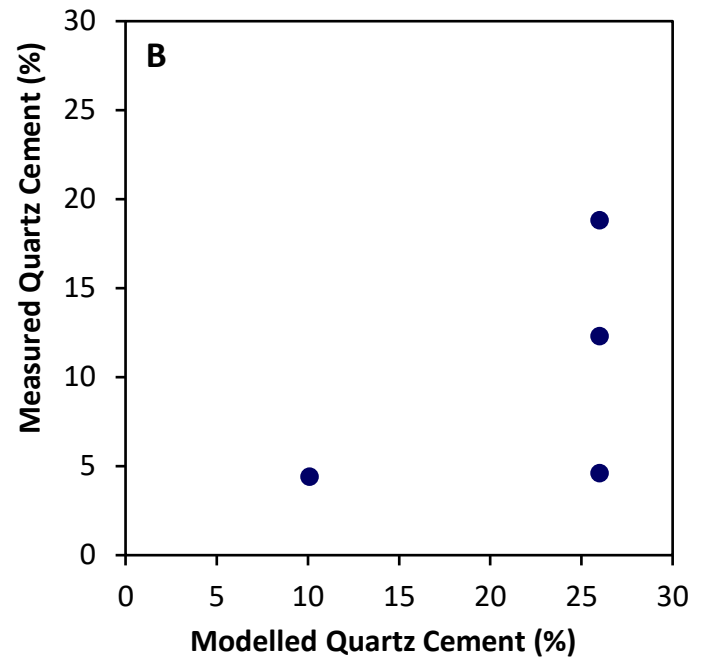
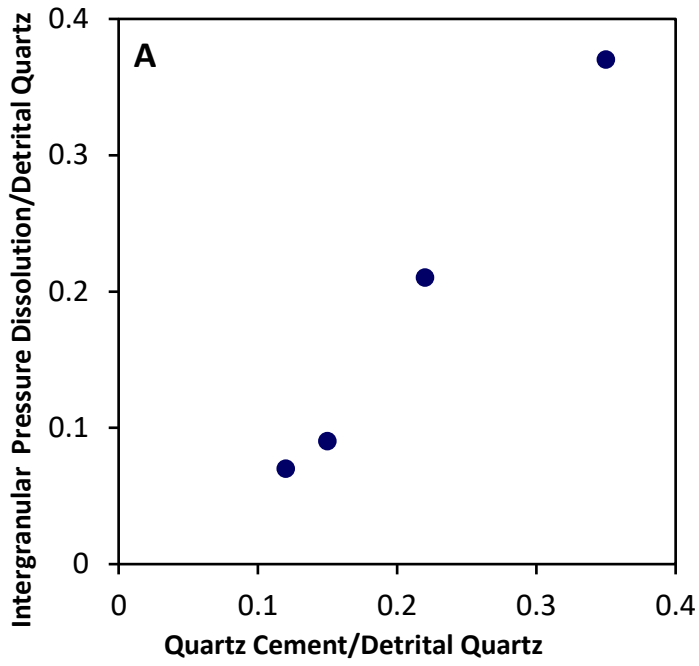
Elgin**Clyde****Lake Creek****Hallson**

Distance from detrital grain boundary (μm)

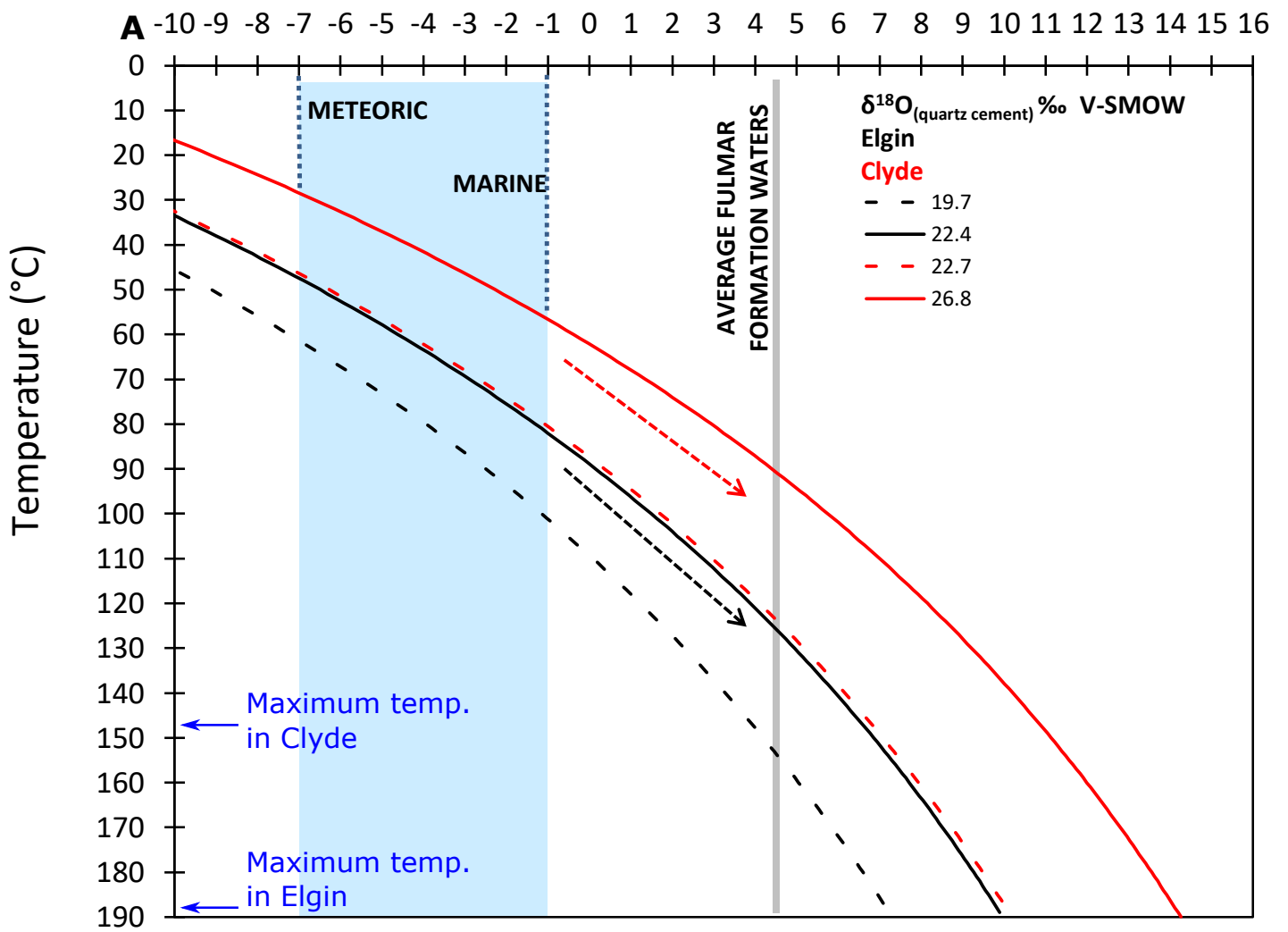


Time spent in quartz cementation window (m.y.)

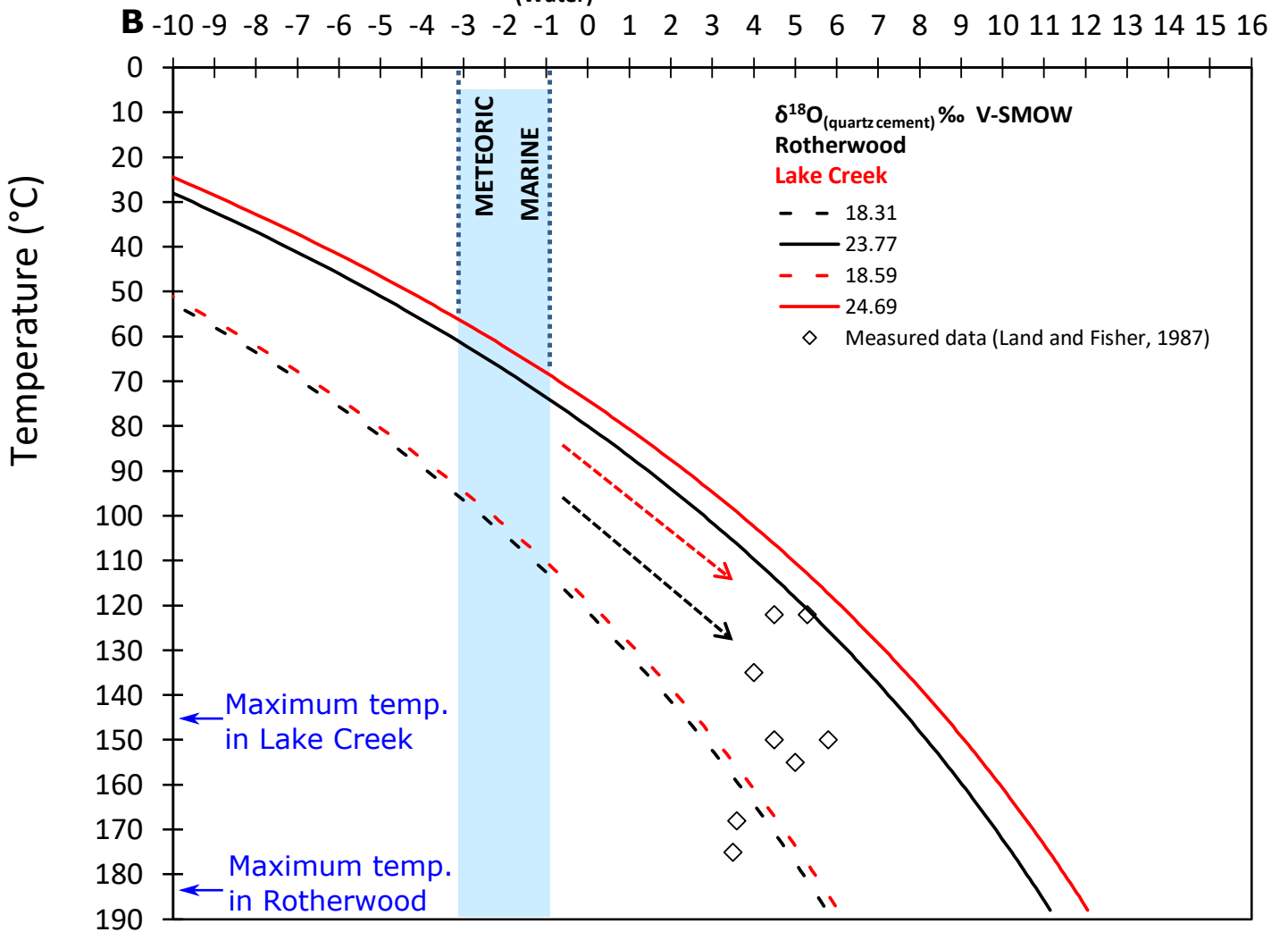
Fraction Quartz Cement

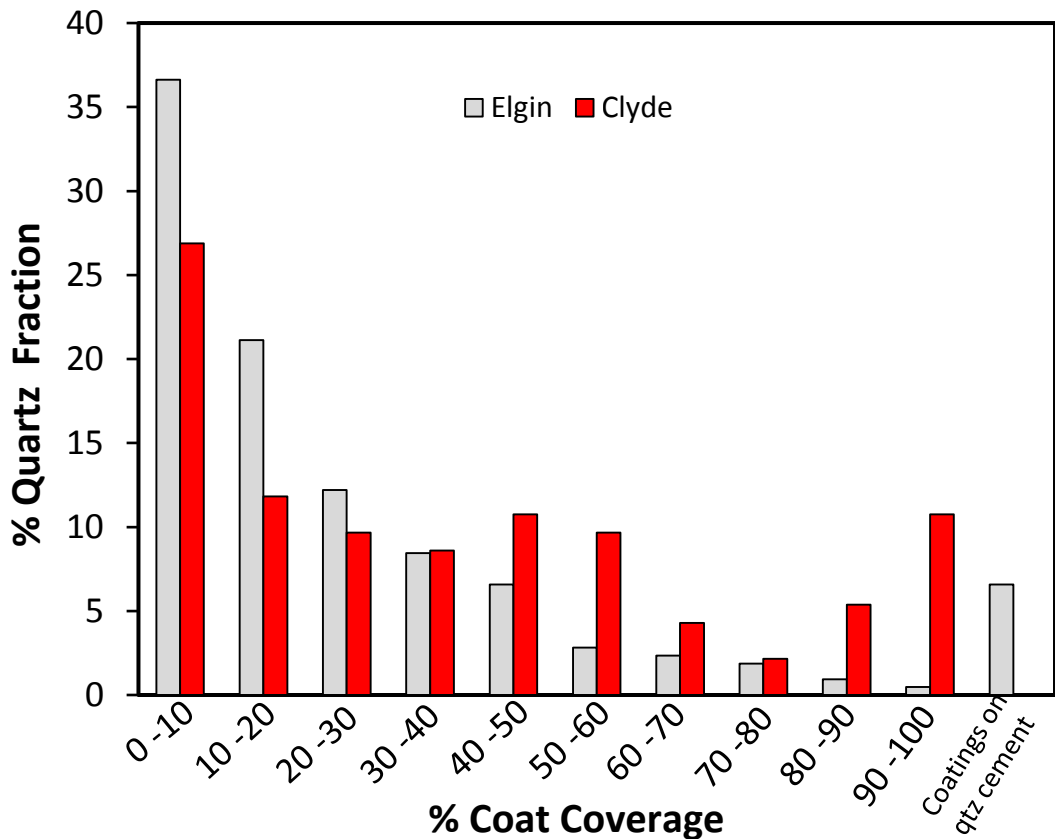


$\delta^{18}\text{O}_{(\text{Water})}$ ‰ V-SMOW



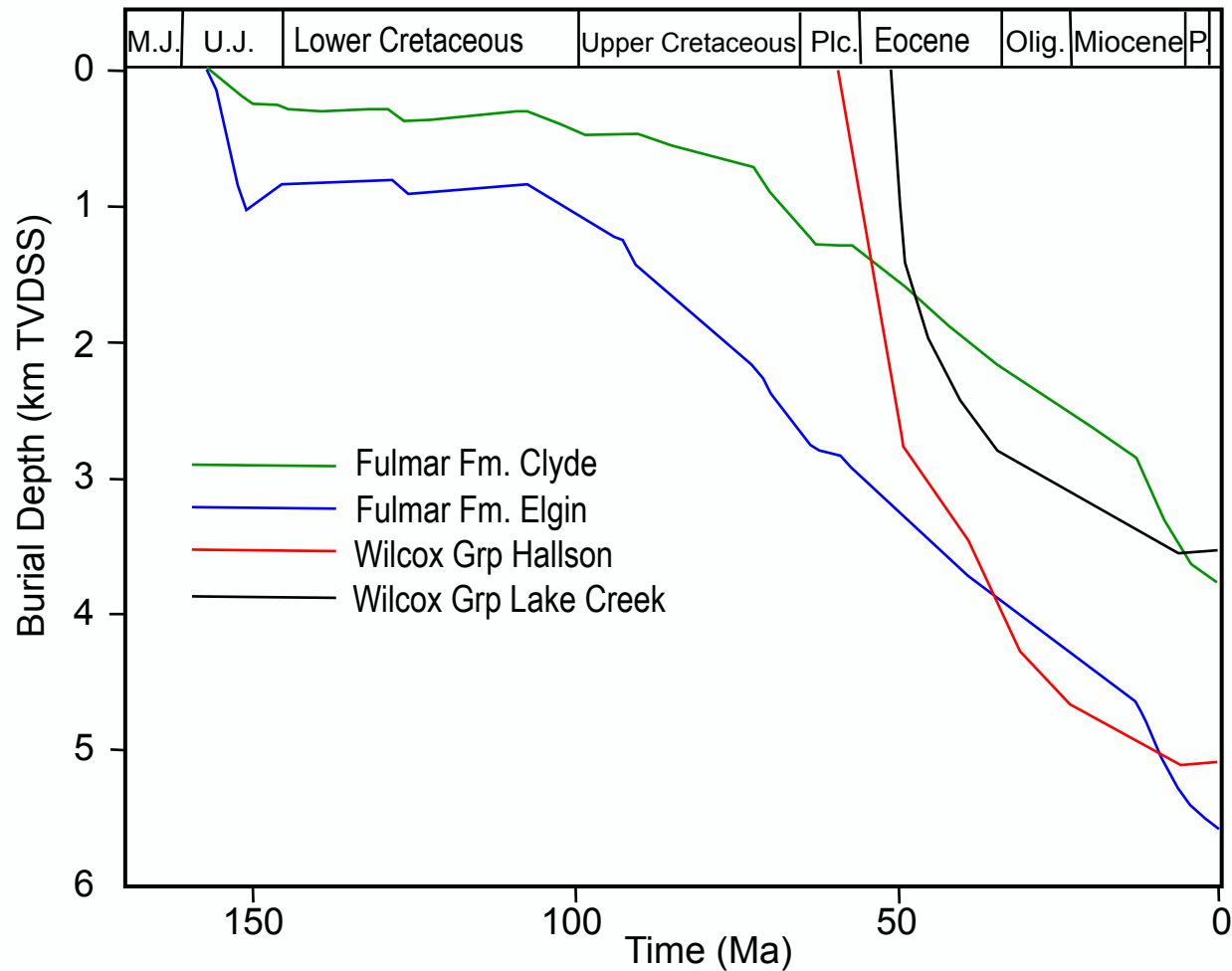
$\delta^{18}\text{O}_{(\text{Water})}$ ‰ V-SMOW

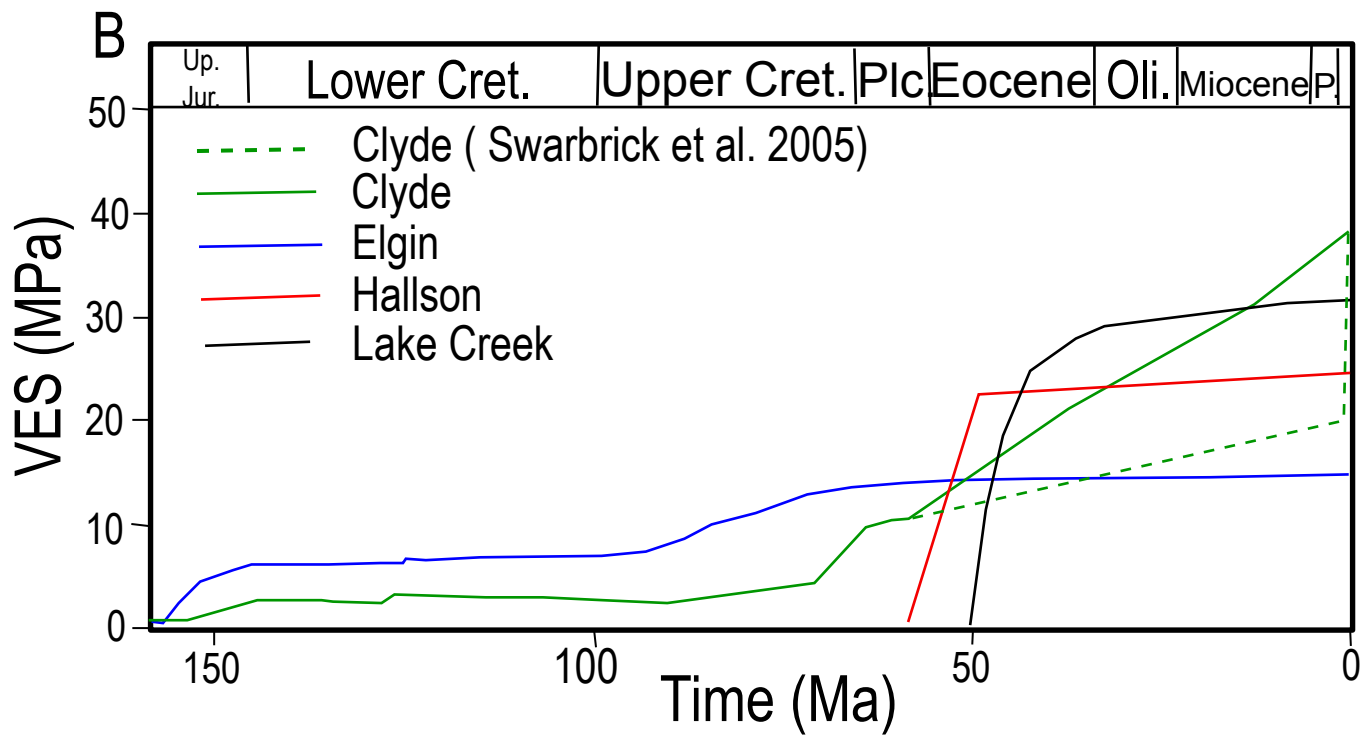
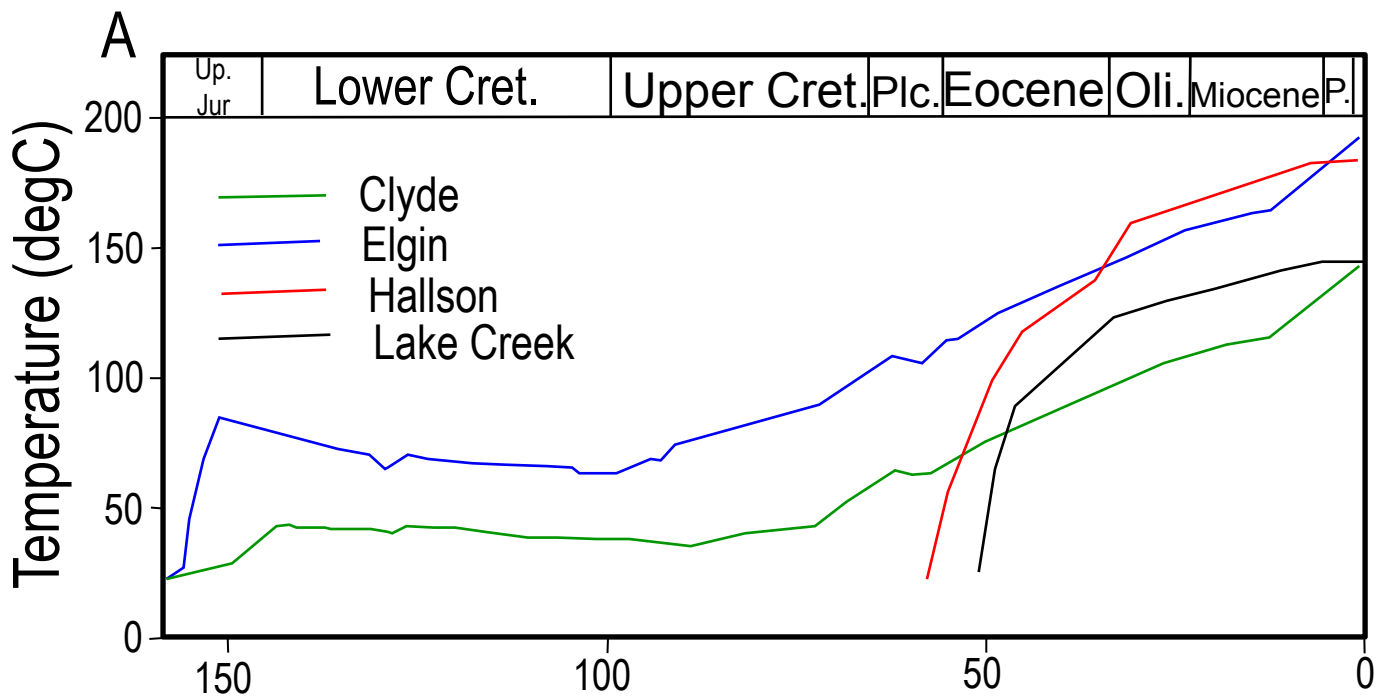


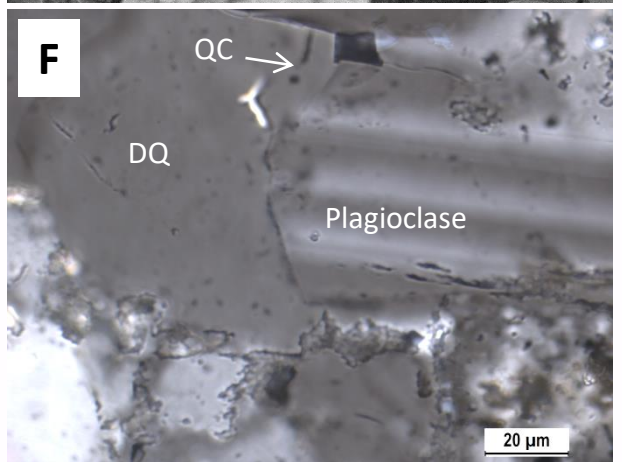
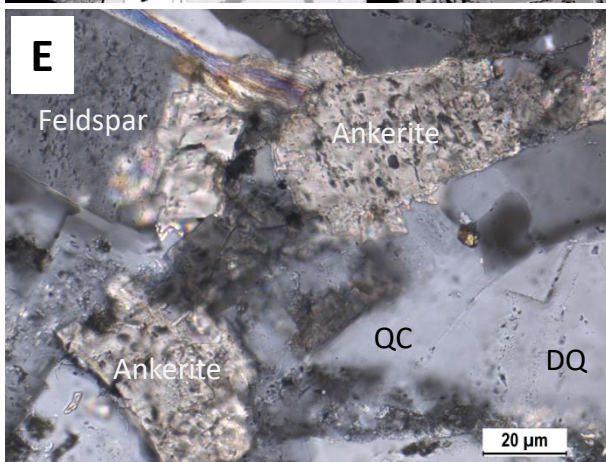
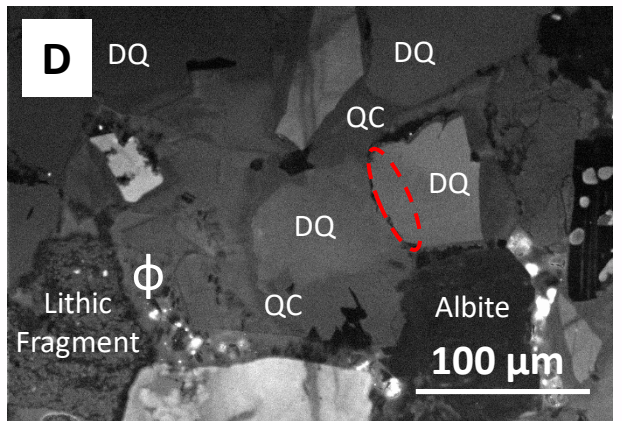
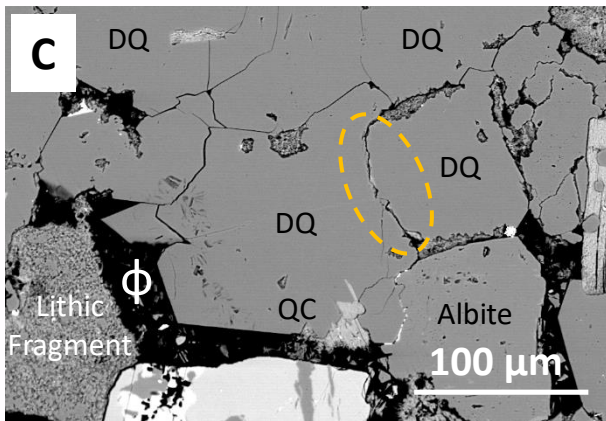
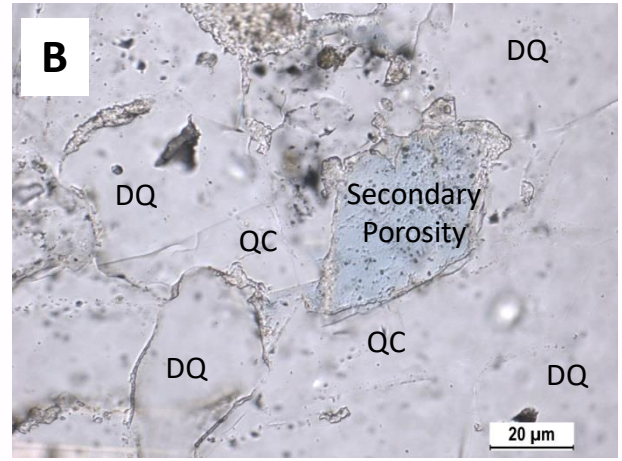
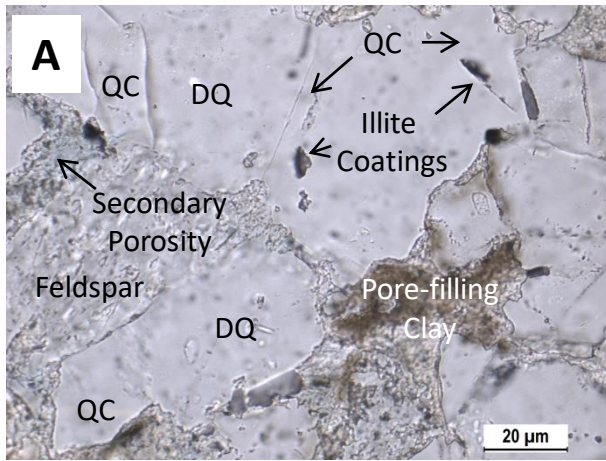


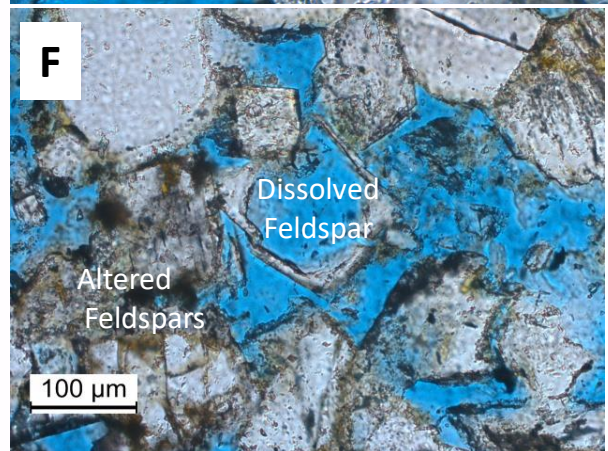
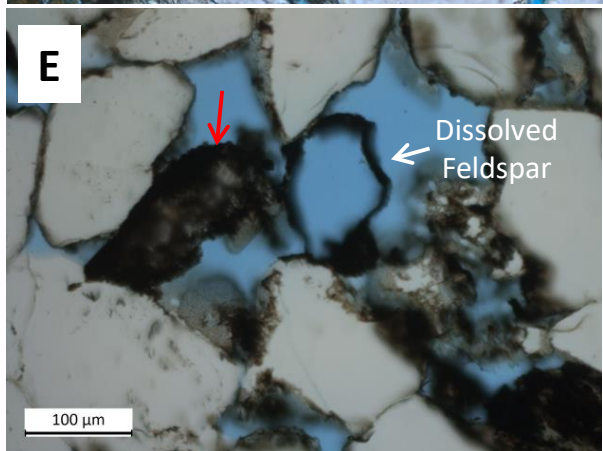
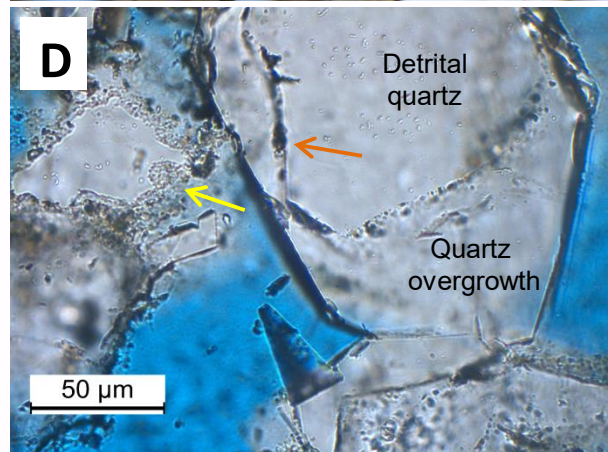
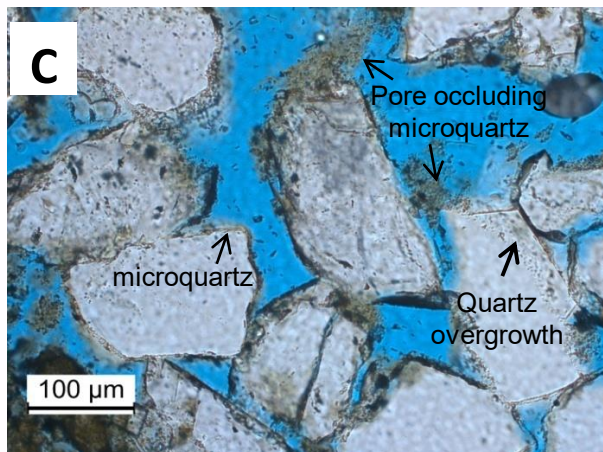
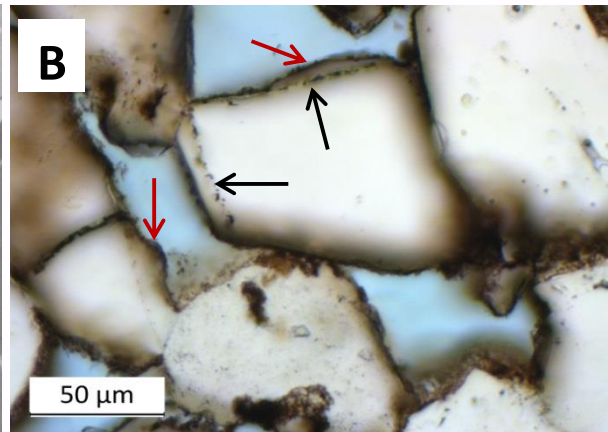
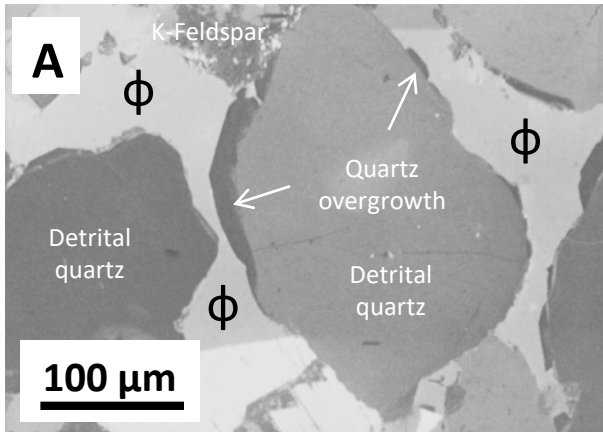
Chrono-Stratigraphy		Lithostratigraphy	
System/ Series	Stage	Stratigraphy	Description
Lower Cret.	Valanginian	Valhall Formation	Marl & Limestone
	Ryazanian		Base Cretaceous Unconformity
Upper Jurassic	Volgian	Kimmeridge Clay Formation	Claystone and Shallow Marine Fulmar Formation Sandstone
	Kimmeridgian	Ribble Sand → Fulmar Formation	
	Oxfordian	Heather Formation	Silty Claystone and Shallow Marine Fulmar Formation Sandstone
Middle Jurassic	Callovian	Pentland Formation	Unconformity Sandstone and Claystone Interbed

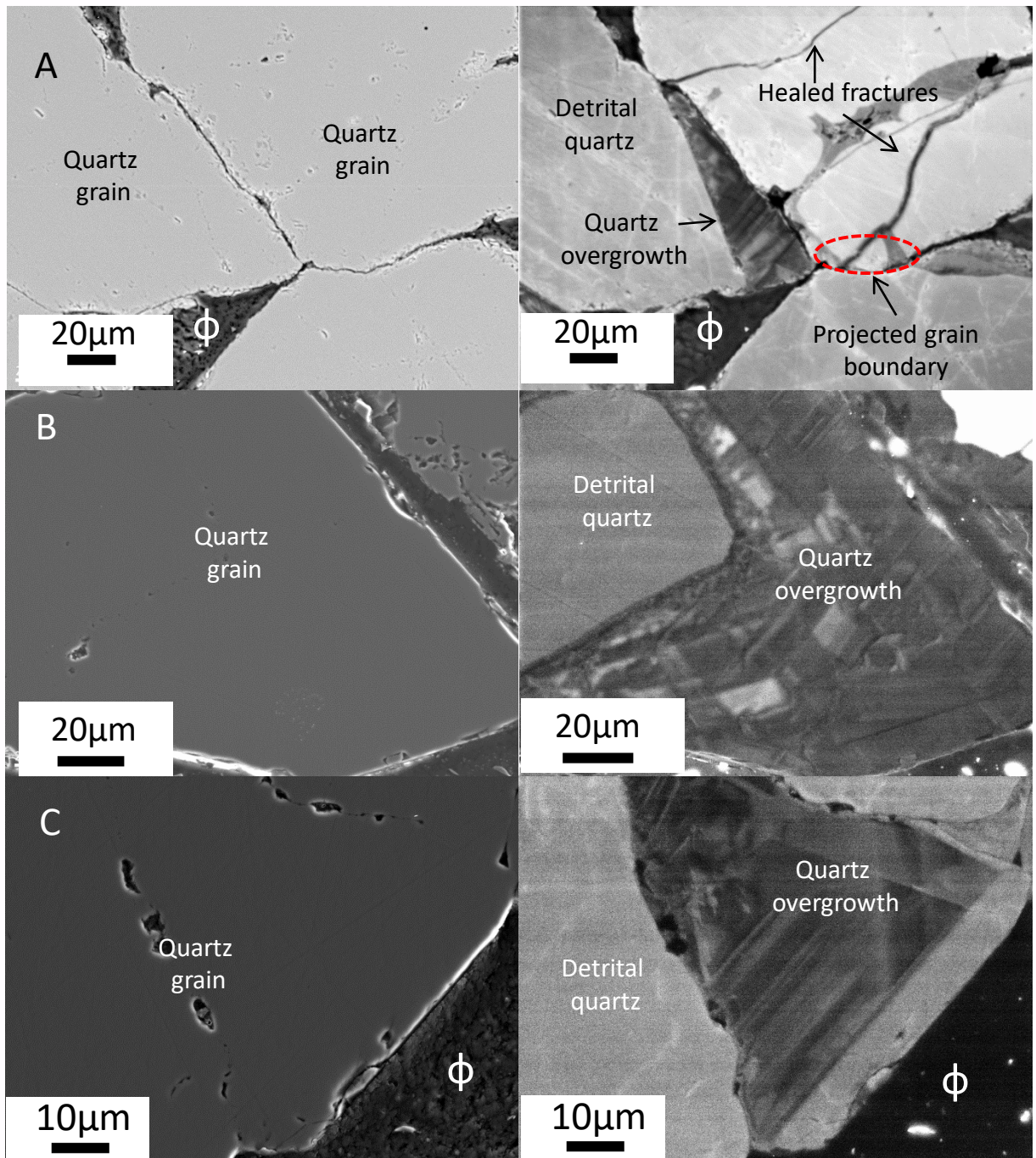
Chronostratigraphy			Lithostratigraphy			
Period	Epoch	Stage	Group or Formation	Description		
Quarter.	Holo-cene Pleisto-cene	Calabrian	Undifferentiated	Predominantly Shale and Sandstone		
Tertiary	Neogene	Piacenzian	Undifferentiated		Shale	
		Zanclean				
	Paleogene	Miocene	Messinian	Fleming	Shale, Siltstone and Sandstone	
			Tortonian			
			Serravallian			
			Langhian			
		Oligocene	Burdigalian	Catahoula		
			Aquitanian			
		Eocene	Chattian	Anahuac		Frio
			Rupelian	Vicksburg		
Priabonian	Jackson					
Bartonian	Claiborne					
Lutetian	Wilcox					
Pale.	Ypresian					
	Thanetian	Midway		Limestone and Marl		
	Seledian					
	Danian					

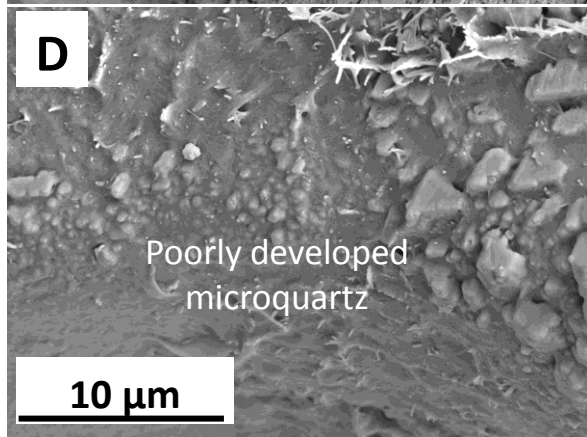
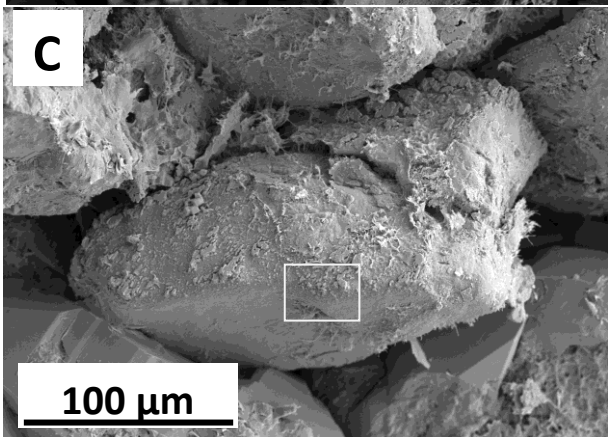
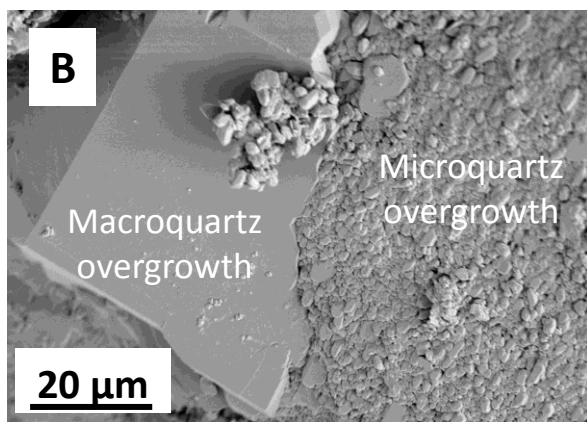
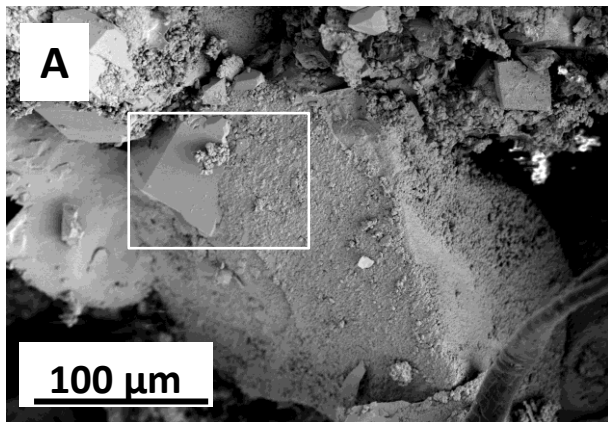












Vertical Effective Stress and Temperature as Controls of Quartz Cementation in Sandstones:
Evidence from North Sea Fulmar and Gulf of Mexico Wilcox Sandstones

Olakunle J. Oye, Andrew C. Aplin, Stuart J. Jones, Jon G. Gluyas, Leon Bowen, Joseph Harwood, Ian J. Orland, and John W. Valley

Highlights

- 12-18 % quartz cement in Wilcox sandstones; 2 - 6% in Fulmar sandstones
- O isotopes suggest quartz forms from 60-80 °C to close to maximum burial temperature
- Most silica for quartz cement can be derived from intergranular pressure dissolution
- Silica supply from IPD may influence rate and extent of quartz cementation
- Consider vertical effective stress history when predicting quartz cement

Declaration of interests

The authors declare that they have no known competing financial interests or personal relationships that could have appeared to influence the work reported in this paper.

The authors declare the following financial interests/personal relationships which may be considered as potential competing interests: